Cuttano *et al.*
Journal of Hematology & Oncology (2022) 15:178
https://doi.org/10.1186/s13045-022-01394-1

Journal of Hematology & Oncology

RESEARCH

Open Access

miRNome profiling of lung cancer metastases revealed a key role for miRNA-PD-L1 axis in the modulation of chemotherapy response

Roberto Cuttano[1], Tommaso Colangelo[1†], Juliana Guarize[2†], Elisa Dama[1], Maria Pia Cocomazzi[1], Francesco Mazzarelli[1], Valentina Melocchi[1], Orazio Palumbo[3], Elena Marino[4], Elena Belloni[5], Francesca Montani[5], Manuela Vecchi[6,7,15], Massimo Barberis[8], Paolo Graziano[9], Andrea Pasquier[10], Julian Sanz-Ortega[11], Luis M. Montuenga[10,12], Cristiano Carbonelli[13], Lorenzo Spaggiari[2,14] and Fabrizio Bianchi[1*]

Abstract

Locally advanced non-small cell lung cancer (NSCLC) is frequent at diagnosis and requires multimodal treatment approaches. Neoadjuvant chemotherapy (NACT) followed by surgery is the treatment of choice for operable locally advanced NSCLC (Stage IIIA). However, the majority of patients are NACT-resistant and show persistent lymph nodal metastases (LNmets) and an adverse outcome. Therefore, the identification of mechanisms and biomarkers of NACT resistance is paramount for ameliorating the prognosis of patients with Stage IIIA NSCLC. Here, we investigated the miRNome and transcriptome of chemo-naïve LNmets collected from patients with Stage IIIA NSCLC ($N = 64$). We found that a microRNA signature accurately predicts NACT response. Mechanistically, we discovered a miR-455-5p/PD-L1 regulatory axis which drives chemotherapy resistance, hallmarks metastases with active IFN-γ response pathway (an inducer of PD-L1 expression), and impacts T cells viability and relative abundances in tumor microenvironment (TME). Our data provide new biomarkers to predict NACT response and add molecular insights relevant for improving the management of patients with locally advanced NSCLC.

Keywords: Lung cancer, NSCLC, microRNA, Gene expression, Chemotherapy, PD-L1, miR-455-5p

Background

Lung cancer is frequently diagnosed as advanced-stage disease (Stage III–IV) with metastases spread to regional and distant organs in more than two-thirds of cases [1]. Despite the progress made in early diagnosis and treatment, the prognosis of patients remains poor with 5-year survival rates ranging from 32 to 6%, depending on the presence of regional or distant metastases, respectively [1]. One-third of patients with non-small cell lung cancer (NSCLC), i.e., the most common type of lung cancer (~80–85% of cases), are diagnosed with locally advanced disease (Stage III). Stage III disease is heterogeneous both for tumor size (from <3 cm, T1; to >7 cm, T4) and for metastatic spreading (i.e., regional lymph nodes, N2-N3; ipsilateral peribronchial and/or ipsilateral hilar lymph nodes and intrapulmonary

†Tommaso Colangelo and Juliana Guarize have contributed equally to this work

*Correspondence: f.bianchi@operapadrepio.it

[1] Unit of Cancer Biomarkers, Fondazione IRCCS Casa Sollievo della Sofferenza, Viale Padre Pio 7, 71013 San Giovanni Rotondo, FG, Italy
Full list of author information is available at the end of the article

nodes, N1) [2]. Stage IIIA-N2 disease is prevalent and, when resectable, is preferentially treated by neoadjuvant chemotherapy (NACT; platinum-based doublet (P-doublet)) before surgery to target nodal metastases and reduce/eradicate metastatic disease. Indeed, NACT is an effective treatment in N2 patients improving the overall survival by 5% at 5 years [3]. However, clinical responses to NACT differ widely, ranging from patients achieving complete eradication of all nodal metastases at the time of surgery (pN0) to patients having a persistent metastatic disease (pN+) [4–6], which suggests the presence of different molecular features among and within nodal metastatic lesions, as recently described also in other studies [7, 8]. Recently, the combination of immune checkpoint inhibitors (ICI) targeting the PD-1/PD-L1 axis (i.e., Nivolumab) with P-doublet chemotherapy in the neoadjuvant setting, showed improved clinical management of patients with resectable NSCLC [9] and gained approval by Food and Drug Administration (FDA). In addition, other ongoing clinical trials are also evaluating the efficacy of ICI alone or in combination with NACT for stage IIIA-N2 NSCLC patients [10]. Nevertheless, the current scant knowledge of the molecular biology of metastases makes it difficult to search for cancer driver mechanisms alongside the development of predictive biomarkers and new druggable targets.

Here, by exploring the miRNA-mRNA transcriptional network of lung cancer lymph node metastases in stage IIIA-N2 disease, we derived miRNA signatures predictive of NACT response. Importantly, using in vitro and in vivo lung cancer models, we showed for the first time the role of miR-455-5p in mediating chemotherapy resistance and immune evasion by means of PD-L1 expression regulation.

Results

Lung cancer metastatic cells exhibit a distinct miRNA profile according to their sensitivity to NACT

We initially investigated the molecular profile of tumor metastatic cells from mediastinal lymph nodes (i.e., LNmets; station 4 and 7; see method) collected by endobronchial ultrasound transbronchial needle aspiration (EBUS-TBNA) before NACT in treatment naïve stage IIIA patients who had a complete pathological response (pN0; $n=5$) or with persistent disease (pN2; $n=7$) after P-doublet NACT (i.e., EBUS samples; Table 1). LNmets were expanded in cell culture (Fig. 1A) as we previously showed [11]; morphological examination together with immunofluorescence staining using anti-pan-cytokeratin antibody (Pan-CK) confirmed their epithelial origin (Fig. 1B). Yet, LNmets were enriched in the expression of typical markers of cells constituting the airway epithelium (*NKX2-1*, *KRT5*, *CC10*, *SOX2*, *SFTPC*; Fig. 1C). Next, we performed high-throughput microRNA expression profiling of LNmets by TaqMan Low-density Array (TLDA; see Methods) and we detected a total of 197 miRNAs (Cqn < 30.01 in at least 50% of samples for group; see Methods) (Fig. 1D-E; Additional file 1: Data File 1). Overall, many miRNAs were downregulated in patients who developed pN2 disease ($n=87$, 44.9%; FC < 0.67) (Fig. 1F), with 16 miRNAs (aka, LN-signature) statistically significant ($p<0.05$) (Fig. 1F-G). TLDA analysis of LNmets in a second independent FFPE cohort of stage III patients ($n=52$) collected by mediastinoscopy (i.e., MED samples; Table 2; Additional file 5: Fig. S1A; see Methods) resulted in the detection of 170 miRNAs (Additional file 5: Fig. S1B), largely overlapping with those identified in EBUS samples (Additional file 5: Fig. S1C) and with a comparable expression level (Additional file 5: Fig. S1D). Again, we observed a general loss of miRNA expression in patients who developed pN2 disease (Additional file 5: Fig. S1E-F). Unsupervised clustering analysis using the LN-signature discriminated pN0 from pN2 also in this independent cohort of patients (Fig. 2A), while partial responder patients (pN1), in line with their intermediate phenotype, resulted to be scattered along the cluster (Fig. 2A). Notably, MED samples showed a similar epithelial cell content as in EBUS samples though

Table 1 Clinical–pathological characteristics of EBUS cohort

	ALL ($n=12$)	pN0 ($n=5$)	pN2 ($n=7$)
Age (years)			
Median (Q1;Q3)	67 (62;72)	69 (66;74)	64 (57;72)
Gender			
Female	5 (42%)	2 (40%)	3 (43%)
Male	7 (58%)	3 (60%)	4 (57%)
Histology			
LUAD	8 (67%)	3 (60%)	5 (71%)
LUSC	4 (33%)	2 (40%)	2 (29%)
Stage			
IIIA	12 (100%)	5 (100%)	7 (100%)
NACT regimen			
CDDP + GEM	10 (83%)	5 (100%)	5 (71%)
CBDCA + GEM	1 (8%)	0 (0%)	1 (14%)
NA	1 (8%)	0 (0%)	1 (14%)
Number of NACT cycles			
3 cycles	8 (67%)	2 (40%)	6 (86%)
4 cycles	3 (25%)	3 (60%)	0 (0%)
NA	1 (8%)	0 (0%)	1 (14%)

Percentages could not add up to 100% due to rounding

LUAD lung adenocarcinoma, *LUSC* lung squamous cell carcinoma, *NACT* neoadjuvant chemotherapy, *CDDP* cisplatin, *GEM* gemcitabine, *CBDCA* carboplatin, *NA* no available data

with a stronger expression of markers of the tumor microenvironment (TME) (*CDH5*, *PTPRC aka CD45,* and *ACTA-2*) (Fig. 2B) which, on the contrary, were absent in pure epithelial LNmets (EBUS samples). Yet, 12 out of the 16 miRNAs of the original LN-signature were also found differentially expressed in MED samples (pN2 vs. pN0; $p < 0.05$) (Fig. 2C and Additional file 5: Fig. S1G). Ridge-penalized logistic regression using the LN-signature (16-miRNA model) resulted in a perfect separation of responders and non-responders in the EBUS cohort when used as a training set, which slightly decreased in the MED cohort used as a validation set (AUC = 0.76) (Fig. 2D–E, Additional file 17: Table S1). When only miRNAs detected in MED samples were used (14-miRNA model), the model reached an AUC = 0.82 in the validation set (Fig. 2D and F, Additional file 17: Table S1). Lastly, as small numbers of biomarkers are easier to use in the clinical practice, we applied LASSO regression which identified a signature of 4 miRNAs (4-miRNA model) with an AUC of 0.81 in the validation set (Fig. 2D and G, Additional file 17: Table S1). Importantly, the clinical model alone, built by combining all available clinical and pathological parameters, showed an AUC of 67% in the validation set which increased up to 82% when combined with miRNA-based risk models (Table 3). Collectively, these results showed a distinct pattern of miRNA expression in LNmets which is predictive of chemotherapy response.

Functional analysis of predictive microRNAs to NACT response

We then used the LN-signature to identify mechanisms of chemotherapy resistance. First, we analyzed public drug screening datasets, such as CTRPv2, GDSC1-2 and PRISM [12–16], to retrieve cisplatin (i.e., the backbone component of NACT) sensitivity data in NSCLC cell lines for which miRNA expression data were available (CCLE dataset). Unexpectedly, the cytotoxic effect of cisplatin was negligible in the majority of the cell lines at the indicated doses (Fig. 3A, Additional file 18: Table S2). However, we noticed that, at least in the GDSC2 dataset, DMSO was used as a compound vehicle, which is known to rapidly inactivate cisplatin [17]. Therefore, we performed a small-scale drug screening to test cisplatin sensitivity (dissolved in NaCl 0.9%) of a panel of metastatic NSCLC cell lines. Cells were treated with increasing doses of cisplatin and drug sensitivity was measured by sigmoidal curve fitting (Fig. 3B). NSCLC cell lines exhibited a heterogeneous sensitivity profile to cisplatin, with potency (IC_{50}) ranging from 1.5 to 11 μM and efficacy (E_{max}) calculated at the peak plasma concentration of cisplatin upon injection (Cmax, ~12 μM: [18, 19]) from 0 to 0.5 relative cell viability (Fig. 3C). When we analyzed the expression of our LN-signature in chemo-naïve NSCLC cell lines, we observed a variable degree of association between IC_{50}/E_{max} values and miRNAs expression (Fig. 3D). Interestingly, miR-455-5p was the top scoring in terms of negative correlation to cisplatin IC_{50}/Emax values ($IC_{50,}$ $r = -0.82$ $p = 0.034$; E_{max}, $r = -0.71$ $p = 0.088$) (Fig. 3D–E). As shown above, this was in line with the downregulation of miR-455-5p observed in LNmets of NACT-resistant patients (Fig. 3F). We also scored a negative correlation for miR-140-3p ($IC_{50,}$ $r = -0.76$ $p = 0.037$; E_{max}, $r = -0.69$ $p = 0.069$) whose overexpression was indeed shown to sensitize NSCLC cells to cisplatin [20, 21] (Fig. 3D).

miR-455-5p regulates cisplatin resistance of lung cancer metastatic cells

Next, we investigated whether miR-455-5p was sufficient to modulate the chemotherapy response of NSCLC cells. To this end, we took advantage of the NCI-H1993 cell line which *i)* was derived from LNmets of a stage IIIA NSCLC patient, *ii)* is a miR-455-5p low-expressing cell line and *iii)* has a higher resistance to cisplatin (Fig. 3E). NCI-H1993 cells were transfected with a miR-455-5p mimic (OE) or a negative mimic control (CTRL) and the increased levels of miR-455-5p after overexpression were confirmed by qRT-PCR

(See figure on next page.)

Fig. 1 miRNA expression profiling of LNmets collected by EBUS-TBNA. **A** Strategy used for miRNA expression profiling of LNmets NSCLC cells (EBUS samples). **B** *Upper panels:* bright-field images of three representative primary LNmets cell lines obtained as described in (**A**). Scale bar, 100 μm. *Lower panels:* representative confocal analysis of pan-cytokeratins (PanCK) in LNmets cell lines. Pan-cytokeratins (red) identify epithelial cells; DAPI (light blue) visualizes nuclei. Scale bar: 50 μm. **C** Heat map showing qRT-PCR results of airway cell markers in five individual LN-metastatic cell lines. Two commercial lung cancer cells (LC; yellow) established from LNmets of stage IIIA NSCLC patients (NCI-H2023 and NCI-H1993) were used as positive controls for airway markers expression, while the breast cancer cells (BC; orange) MDA-MB-231 and leukemic cells (LK; magenta) HL-60 were used as negative controls. Data are log_2-ratio. **D** Bar plot showing the number and percentage of miRNAs detected (yellow) or not detected (blue) in EBUS samples. **E** Violin plot showing expression levels (Cqn) of all miRNAs detected in EBUS samples. **F** Volcano plot showing differentially expressed miRNAs in chemoresistant (pN2; $N = 7$) vs. chemosensitive (pN0; $N = 5$) LNmets. Gray dot, unchanged; blue dot, downregulated ($p < 0.05$); red dot, upregulated ($p < 0.05$); statistical significance was calculated using the Mann–Whitney *U* test. **G** Hierarchical clustering analysis of differentially expressed miRNAs ($N = 16$, aka LN-signature) in pN2 vs pN0 LNmets. Data are log_2-ratio. LUAD, lung adenocarcinoma; LUSC, lung squamous cell carcinoma

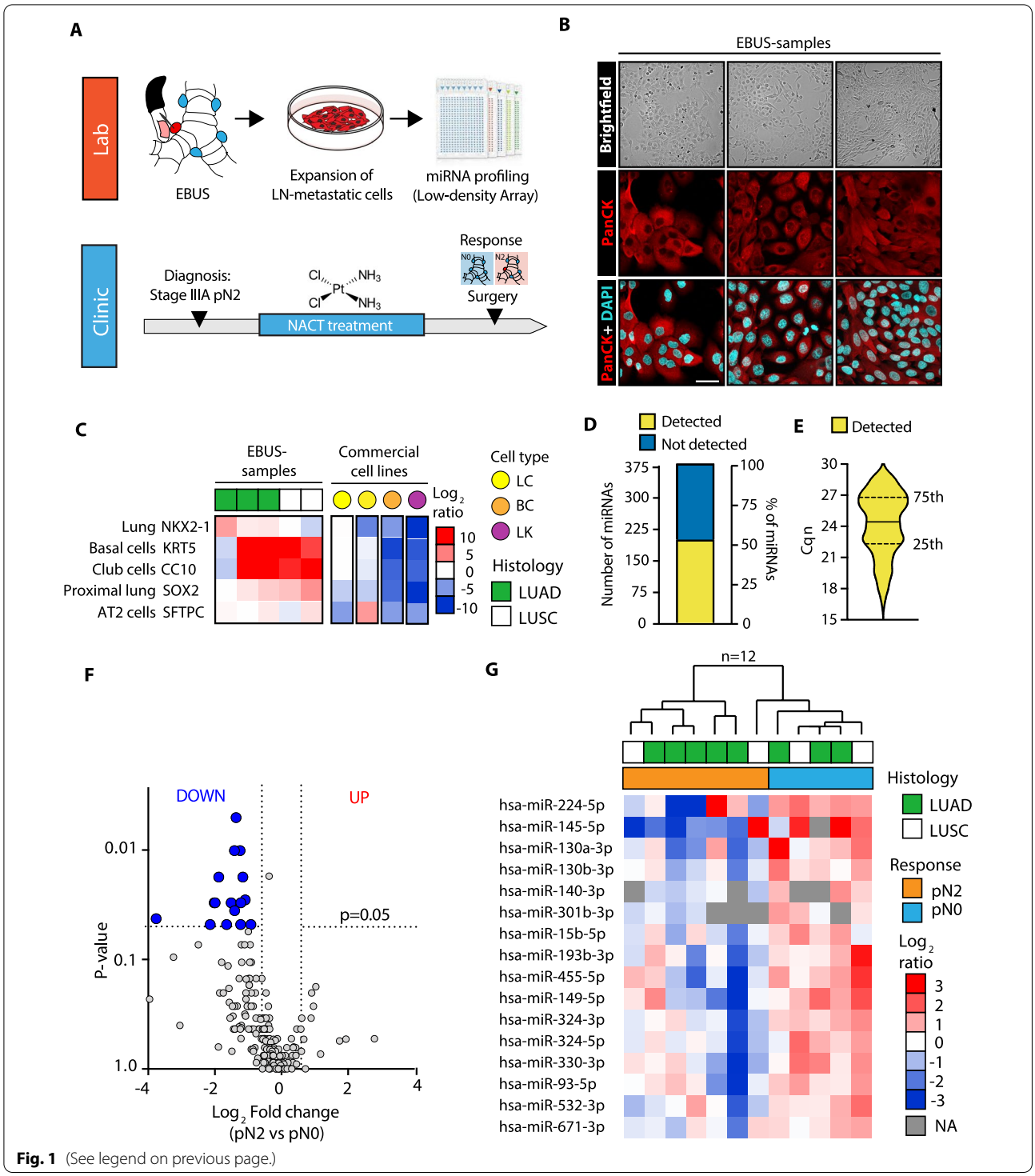

Fig. 1 (See legend on previous page.)

(Fig. 4A). Importantly, we observed that miR-455-5p OE in NCI-H1993 strongly increased sensitivity to cisplatin (Fig. 4B) with a significant decrease in cisplatin potency in comparison with CTRL cells (Fig. 4C). We then investigated whether miR-455-5p could play a role also in acquiring cisplatin resistance and thus we treated the cisplatin sensitive NCI-H2023 cell line (Fig. 3C) with increasing doses of cisplatin during cycles of drug on (4 days) and drug off (1–2 weeks) (Fig. 4D). Long-term treatment with cisplatin resulted in the generation of

Table 2 Clinical–pathological characteristics of MED cohort

	ALL ($n=52$)	pN0 ($n=10$)	pN2 ($n=32$)	pN1 ($n=10$)
Age				
Median (Q1;Q3)	62.12 (59.18; 68.24)	62.05 (59.81; 70.32)	61.32 (58.82; 66.97)	62.95 (59.86; 66.32)
Gender				
Female	15 (28.8%)	3 (30%)	9 (28.1%)	3 (30%)
Male	37 (71.2%)	7 (70%)	23 (71.9%)	7 (70%)
Histology				
LUAD	30 (57.7%)	4 (40%)	22 (68.7%)	4 (40%)
LUSC	19 (36.5%)	4 (40%)	9 (28.1%)	6 (60%)
NSCLC	3 (5.8%)	2 (20%)	1 (3.1%)	0 (0%)
Stage				
IIIA	46 (88.5%)	8 (80%)	29 (90.6%)	9 (90%)
IIIB	6 (11.5%)	2 (20%)	3 (9.4%)	1 (10%)
NACT regimen				
CDDP + ALIMTA	6 (11.5%)	0 (0%)	5 (15.6%)	1 (10%)
CDDP + GEM	41 (78.8%)	9 (90%)	25 (78.1%)	7 (70%)
CDDP + TAXOTERE	1 (1.9%)	0 (0%)	1 (3.1%)	0 (0%)
CDDP + VNR	4 (7.7%)	1 (10%)	0 (0%)	2 (20%)
VNR + GEM	1 (1.9)	0 (0%)	1 (3.1%)	0 (0%)
Number of NACT cycles				
2–3 cycles	42 (80.8%)	9 (90%)	24 (75%)	9 (90%)
4–5 cycles	9 (17.3%)	1 (10%)	7 (25%)	1 (10%)

Percentages could not add up to 100% due to rounding

LUAD lung adenocarcinoma, *LUSC* lung squamous cell carcinoma, *NSCLC* other non-small cell lung subtypes, *NACT* neoadjuvant chemotherapy, *CDDP* cisplatin, *GEM* gemcitabine, *CBDCA* carboplatin, *VNR* vinorelbine, *NA* no available data

a resistant variant of the NCI-H2023 cell line namely the NCI-H2023-CDDP-R (aka, CDDP-R), which was characterized by a significant increase in both IC_{50} and E_{max} in comparison with parental cells (Additional file 6: Fig. S2A-B). The acquirement of resistance to cisplatin was accompanied by the acquisition of a typical elongated cell shape (Additional file 6: Fig. S2C), an increased mRNA and protein expression of epithelial-to-mesenchymal transition (EMT) master regulators (i.e., ZEB1, SLUG and TWIST1) and of mesenchymal/stem cells markers (VIM, ACTA-2, CD90) (Additional file 6: Fig. S2D-F) [22]. Indeed, the gene expression profiling of parental and CDDP-R cells (Additional file 6: Fig. S2G) followed by gene set enrichment analysis (GSEA) using 'Hallmark genes set' collection, revealed that the 'EMT gene signature' was the highest one significantly enriched in cisplatin-resistant cells (Additional file 6: Fig. S2H-I, Additional file 19: Table S3A). Lastly, we observed a reduced proliferation rate and a higher migratory/invasive capability of CDDP-R cells (Additional file 6: Fig. S2J-L).

In line with the above observations, miR-455-5p was significantly downregulated after the acquisition

(See figure on next page.)

Fig. 2 LN-signature predicts chemotherapy response of chemo-naïve lung metastatic tumor tissue collected by mediastinoscopy. **A** Hierarchical clustering analysis of the LN-signature in MED samples. Data are log_2-ratio. LUAD, lung adenocarcinoma; LUSC, lung squamous cell carcinoma; NSCLC, other non-small cell lung subtypes; NA, no available data. **B** Heat map showing gene expression of the indicated marker analyzed by qRT-PCR in LNmets (EBUS samples, $N=5$; and MED samples, $N=5$). NCI-H2023 and NCI-H1993 lung cancer cells (LC, yellow) were used as positive controls for the expression of epithelial marker, while HUVEC (EN, orange), WI38 (FI, red) and HL-60 cells (LK, magenta) were used as positive control for endothelial, fibroblast and immune-like markers expression, respectively. Data are log_2-ratio. **C** Pie chart showing the number of miRNAs of LN-signature ($N=16$) that were found differentially expressed between pN0 and pN2 samples in MED cohort. **D** Schematic representation of strategy adopted to derive miRNA-based NACT-predictive models. **E**–**G** *Upper panels:* receiver operating characteristic (ROC) curves of the 16-miRNA model (**E**), 14-miRNA model (**F**) and 4-miRNA model (**G**) in the validation set (MED samples, red). *Lower panels*: box plot of the predicted probability of being a responder according to the 16-miRNA model (**E**), 14-miRNA model (**F**) and 4-miRNA model (**G**)

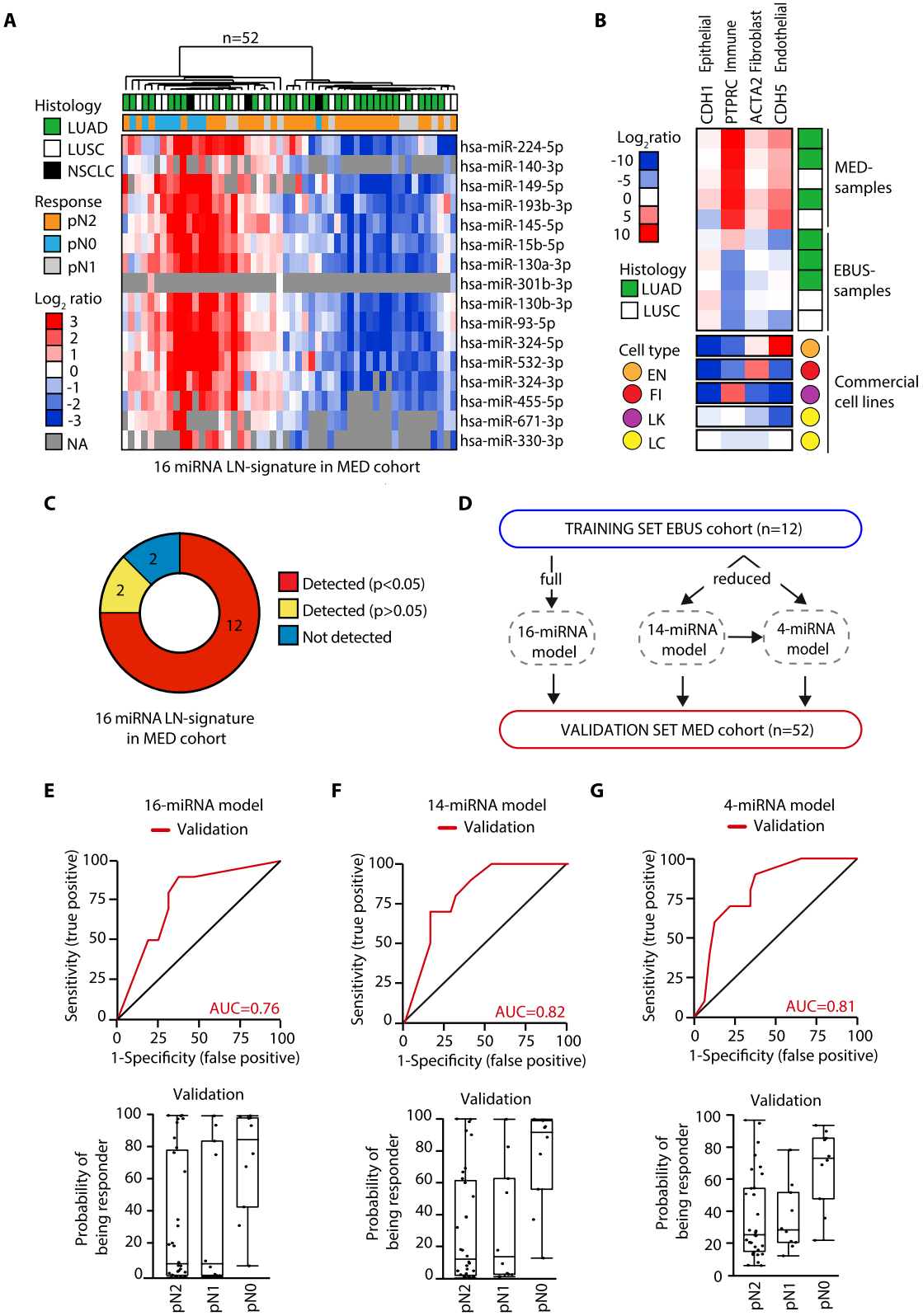

Fig. 2 (See legend on previous page.)

Table 3 Combination of clinical model with miRNA predictive model in MED cohort

MED cohort (validation set)	OR (95% CI)	Wald *p* value	AUC (%)
(A)			
Clinical model			
Age (5-unit increase)	1.04 (0.65–1.66)	0.88	
Gender (male vs. female)	0.58 (0.10–3.31)	0.54	67
Histology (LUSC/NSCLC NOS vs. LUAD)	3.88 (0.79–19.18)	0.1	
miRNA model			
16-miRNA risk score	1.20 (1.00–1.44)	0.046	76
14-miRNA risk score	1.37 (1.07–1.75)	0.013	82
4-miRNA risk score	2.00 (1.17–3.42)	0.012	81
(B)			
Clinical model			
Age (5-unit increase)	1.12 (0.67–1.86)	0.67	
Gender (male vs. female)	0.46 (0.07–2.98)	0.42	
Histology (LUSC/NSCLC NOS vs. LUAD)	2.71 (0.51–14.48)	0.24	77
miRNA model			
16-miRNA risk score	1.19 (0.99–1.45)	0.07	
(C)			
Clinical model			
Age (5-unit increase)	1.13 (0.67–1.93)	0.88	
Gender (male vs. female)	0.40 (0.06–2.78)	0.54	
Histology (LUSC/NSCLC NOS vs. LUAD)	2.40 (0.42–13.79)	0.1	82
miRNA model			
14-miRNA risk score	1.37 (1.06–1.77)	0.018	
(D)			
Clinical model			
Age (5-unit increase)	1.14 (0.67–1.94)	0.63	
Gender (male vs. female)	0.46 (0.07–3.11)	0.42	
Histology (LUSC/NSCLC NOS vs. LUAD)	1.95 (0.33–11.38)	0.46	80
miRNA model			
4-miRNA risk score	1.98 (1.11–3.54)	0.022	

(A) Performance of single predictive models based on clinical information (age, gender or histology) or miRNA expression (16, 14 and 4 miRNAs). (B–D) Combination of clinical models with 16-miRNA risk score (B), 14-miRNA risk score (C) and 4-miRNA risk score (D)

Odds Ratio (OR)

P value calculated by Wald test and AUC of indicated models are reported in the table

of cisplatin resistance in CDDP-R vs. parental cells (Fig. 4E). We, therefore, transfected miR-455-5p in both parental and CDDP-R cells (Fig. 4F) and performed cell viability analysis upon cisplatin treatment (Fig. 4G). Strikingly, miR-455-5p overexpression in CDDP-R cells induced cisplatin sensitivity in terms of both potency and efficacy when compared to parental cells or parental cells overexpressing miR-455-5p (Fig. 4G-H), thus suggesting a specific miR-455-5p-addiction in resistant cells.

We validated such findings also in vivo by using a zebrafish cell-derived xenograft (zCDX) model which was recently shown to be valuable in oncology research [23, 24]. First, parental and CDDP-R cells overexpressing miR-455-5p or not, as a control, were fluorescently labeled and then injected into the perivitelline space of zebrafish larvae (Fig. 4I). qRT-PCR analysis confirmed miR-455-5p OE before cell inoculation (Additional file 7: Fig. S3A). Next, zebrafish embryos were treated with cisplatin at a dose near Cmax (~16 μM) and tumor growth was analyzed (Fig. 4I-J). The implantation rate was 100% in both cell lines upon injection (on day 0), with parental cells that formed slightly smaller tumors when compared to tumors formed by CDDP-R cells (Additional file 7: Fig. S3B-C). The cisplatin treatment induced a significant reduction in the tumor size of the parental tumors but not of the CDDP-R ones (Fig. 4K-L).

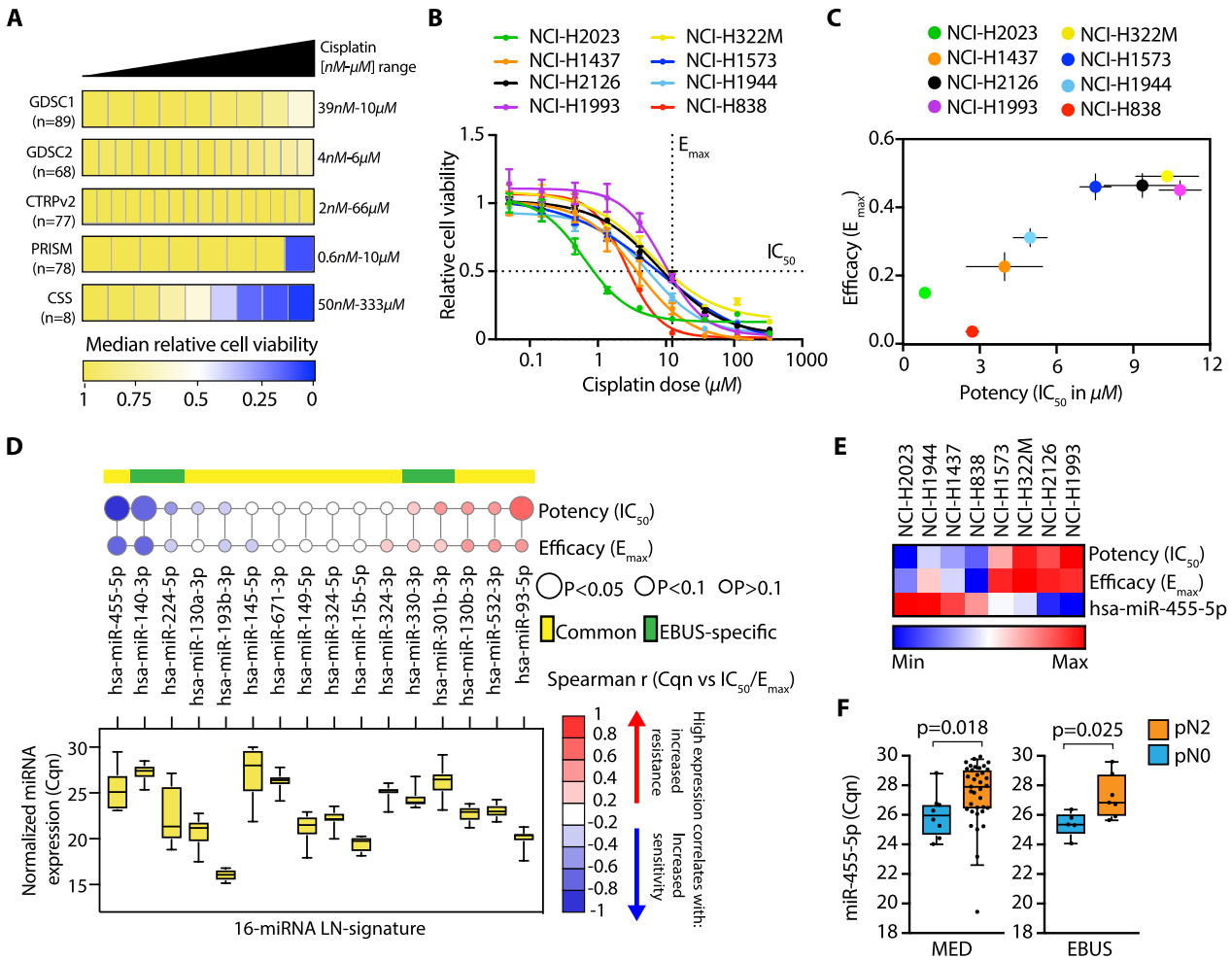

Fig. 3 Basal levels of miR-455-5p negatively correlate with cisplatin resistance in vitro. **A** Heatmap of cell viability values (median normalized) of NSCLC cell lines at increasing concentrations of cisplatin. Heatmap square represents an individual drug concentration drug. For each dataset, the number of cell lines and concentration range used (minimum–maximum) are indicated. **B** Dose–response curves of the indicated NSCLC cell lines treated with cisplatin for 72 h. Error bars indicate SEM ($N = 3$ to 5). **C** Distribution of potency (IC_{50}) versus efficacy values (E_{max}) of cisplatin in the indicated NSCLC cell lines. Data are mean ± SEM (N = 3 to 5). **D** *Upper panel*: bubble plot reporting correlation coefficient (*r*) between basal level of normalized miRNA expression (Cqn) and IC_{50} or E_{max} values. The size of the bubble is proportional to statistical significance calculated by the Spearman correlation test, while colors indicate *r* coefficient. Yellow: common differentially expressed miRNAs in both EBUS and MED samples; green: miRNAs differentially expressed in EBUS samples only. *Lower panel*: box plot representing the expression levels (Cqn) of miRNAs in the panel of NSCLC cell lines. **E** Heatmap of mean value of IC_{50}, E_{max} and miR-455-5p expression (Cqn) in the indicated cell lines. **F** Box plot showing miR-455-5p expression levels (Cqn) in chemoresistant (pN2) and chemoresponsive (pN0) patients in MED and EBUS samples. P values were calculated by the Mann–Whitney U test

Strikingly, miR-455-5p overexpression re-sensitized CDDP-R tumors to cisplatin (Fig. 4K-L). Yet, miR-455-5p OE alone caused a significant reduction in the tumor burden in CDDP-R untreated resistant tumors (Fig. 4K–L). This is in line with in vitro data where miR-455-5p OE impaired tumor cell proliferation (Additional file 8: Fig. S4A–B) and with the observation that high miR-455-5p expressing tumors from TGCA-LUAD cohort are smaller in size when compared to low miR-455-5p ones (Additional file 20: Table S4).

PD-L1 is a direct molecular link between miR-455-5p and cisplatin resistance

We then asked which molecular mechanisms can be influenced by miR-455-5p and their role in cisplatin resistance. To tackle this, we reconstructed miRNA-mRNA transcriptional networks by performing transcriptome analysis of LNmets (MED samples) which identified 1702 differentially expressed genes (DEGs) (fold change > |1.5|; $p < 0.05$) in pN2 vs. pN0 patients (Fig. 5A). GSEA using a curated gene set representing

miR-455-5p-predicted target genes ($n = 349$, Additional file 3: Data File 3; see Methods) revealed a positive enrichment (FDR < 0.05) of miR-455-5p targets in pN2 patients, which was coherent with the previously observed loss of miR-455-5p expression (Fig. 5B). Next, we used the 'Hallmark genes set' collections in GSEA which revealed a number of pathways involved in the regulation of proliferation, metabolism, immune evasion, development and response to cellular stresses, enriched in LNmets of pN2 patients (FDR < 0.05) (Fig. 5C, Additional file 19: Table S3B). To functionally dissect the regulation of pN2-enriched pathways, we transfected NCI-H1993 and CDDP-R cells with a miR-455-5p mimic (OE) or a negative mimic control (CTRL) and performed transcriptome analysis. GSEA confirmed the modulation of miR-455-5p target genes upon miRNA overexpression (Fig. 5B). Strikingly, comparative analysis of significantly enriched 'Hallmark gene sets' (FDR < 0.05) in MED samples and in the two NSCLC cell lines (NCI-H1993 and CDDP-R) revealed that 'INTERFERON-ALPHA (IFN-α) RESPONSE' and 'INTERFERON-GAMMA (IFN-γ) RESPONSE' were overlapping and enriched in LNmets of pN2 patients likewise in low-miR-455-5p expressing NSCLC cell lines with the same trend of regulation (Fig. 5C–E, Additional file 19: Table S3B–D). Next, we looked among genes belonging to IFN-α and IFN-γ response pathways to search for putative miR-455-5p target genes by TargetScan analysis [25]. *BATF2*, *CMPK2*, *IRF2*, *MYD88*, *SOCS3* and *PD-L1* (aka *CD274*) genes were all predicted to be targeted by miR-455-5p (Fig. 5F). Among these genes, PD-L1 expression was previously reported to be found increased after NACT treatment in NSCLC [26–28]. Moreover, besides the well-known role of PD-L1 in the regulation of T cell activity through the interaction with the receptor PD-1, it was also found to regulate critical functions of cancer cells in a cell-autonomous way, including chemotherapy resistance [29, 30]. Therefore, we speculated that miR-455-5p regulation would impact chemotherapy response through PD-L1 direct regulation. Overall, we analyzed PD-L1 expression (mRNA, total and cell surface protein) in our panel of NSCLC cell lines (Additional file 9: Fig. S5A-C) and found that a higher expression of PD-L1 was associated with cisplatin resistance (Additional file 9: Fig. S5D-E). Furthermore, when we silenced PD-L1 expression by siRNAs in NCI-H1993 cells the sensitivity to cisplatin increased significantly (Additional file 9: Fig. S5F-H). Conversely, the acquisition of cisplatin resistance was accompanied by a concomitant increase in PD-L1 expression in CDDP-R when compared to parental cells (Additional file 10: Fig. S6A-C). Accordingly, silencing of PD-L1 by siRNAs in CDDP-R cells (Additional file 10: Fig. S6D) was able to strongly enhance cisplatin sensitivity when compared to control cells (Additional file 10: Fig. S6E-F), whilst no effect was scored in the parental cell lines where PD-L1 expression was low (Additional file 10: Fig. S6E–F).

miR-455-5p/PD-L1 axis contributes to cisplatin resistance in lung metastatic cells

We then searched for predicted miRNA-binding sites in the 3' untranslated region (3'-UTR) of *PD-L1* (aka *CD274*) which revealed a binding site (8-mer) for miR-455-5p (Fig. 5F and 6A). Indeed, we found an inverse correlation between miR-455-5p expression and PD-L1 protein amount in our panel of NSCLC cell lines (Fig. 6B). Yet, PD-L1 mRNA levels were found to be strongly upregulated in LNmets of pN2 (i.e., low miR-455-5p) vs. pN0 (i.e., high miR-455-5p) patients (Fig. 6C). Remarkably, miR-455-5p expression and PD-L1 tumor proportion score showed a trend of inverse correlation also in primary NSCLC from two other independent

(See figure on next page.)

Fig. 4 miR-455-5p modulates cisplatin resistance in vitro and in vivo. **A** qRT-PCR of miR-455-5p in NCI-H1993 transfected with a miR-455-5p mimic (NCI-H1993 OE) or a negative control mimic (NCI-H1993 CTRL). Data, expressed as normalized Cq (Cqn), are mean ± SEM ($N = 5$). *P* value was calculated by the Mann–Whitney U test. **B** Dose–response curves of NCI-H1993 CTRL and NCI-H1993 OE cells treated with cisplatin for 72 h. Error bars indicate SEM ($N = 4$). **C** Bar plot of cisplatin potency and efficacy of NCI-H1993 CTRL and NCI-H1993 OE cells. Data are mean ± SEM ($N = 4$). Fold change is relative to NCI-H1993 CTRL. *P* value was calculated by one sample *t* test. $^*P < 0.05$; ns, not significant. **D** Generation of a model of in vitro acquired cisplatin resistance. **E** qRT-PCR of miR-455-5p in Parental and CDDP-R cell lines. Data, expressed as Cqn, are mean ± SEM ($N = 4$). *P* value was calculated by t test with Welch's correction. **F** qRT-PCR of miR-455-5p in Parental and CDDP-R transfected either with a miR-455-5p mimic (i.e., Parental OE and CDDP-R OE) or a negative control mimic (i.e., Parental CTRL and CDDP-R CTRL). Data, expressed as Cqn, are mean ± SEM ($N = 4$). *P* value was calculated using the Mann–Whitney *U* test. $^*P < 0.05$. **G** Dose–response curves of indicated cell lines treated with cisplatin for 72 h. Error bars indicate SEM ($N = 5$). **H** Bar plot of cisplatin potency and efficacy of Parental CTRL, Parental OE, CDDP-R CTRL and CDDP-R OE cells. Data are mean ± SEM ($N = 5$). Fold change is relative to CTRL. P value was calculated by one sample *t* test. $^{**}P < 0.01$; ns, not significant. **I** Schematic representation of zCDX model to monitor chemotherapy response in vivo. **J** Representative fluorescence images of zebrafish larvae injected with tumor cells. Dil (red) identifies tumor cells; eGFP (green) visualizes blood vessels. Scale bar: 200 µm. **K** Representative fluorescence images of tumor masses upon 3 days of cisplatin treatment. Dil (red) identifies tumor cells. Scale bar: 200 µm. **L** Size distribution of tumor masses derived from indicated cell lines. Columns represent mean ± SEM ($N = 16$–20, for each condition). Results are shown as relative tumor size (i.e., percent change in tumor size by comparing day 4 vs. day 1). Effect size is expressed as percent reduction in mean value of tumor size. P values were calculated by the Mann–Whitney *U* test

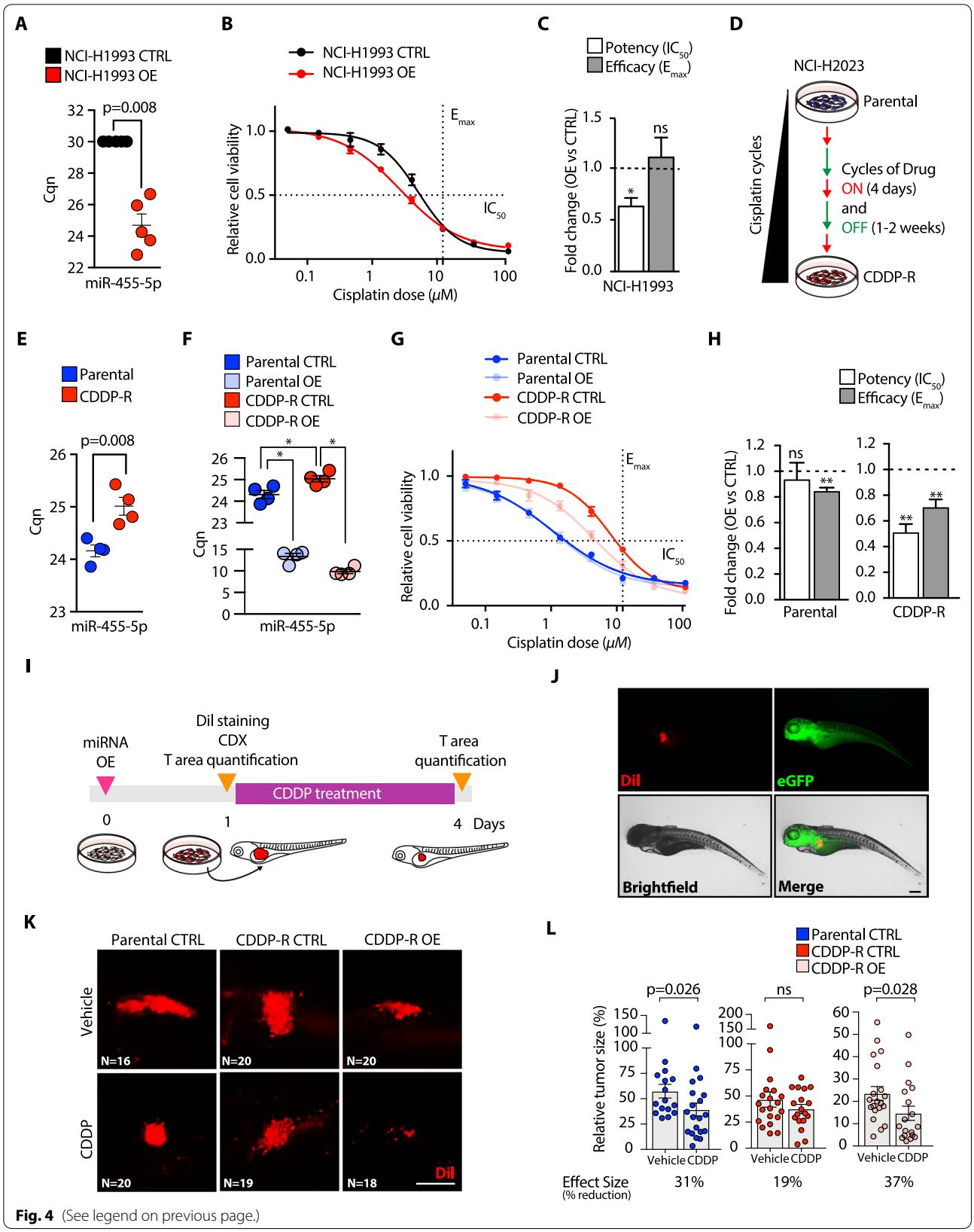

Fig. 4 (See legend on previous page.)

cohorts of patients (the CSS and CIMA-CUN cohorts; Additional file 21: Table S5; Fig. 6D, E). We also analyzed miRNA- and RNA-seq data from the TGCA-LUAD and TGCA-LUSC cohorts ($N_{LUAD}=507$, $N_{LUSC}=473$; Fig. 6F). When tumor samples were stratified based on the miR-455-5p expression level ('High,' 'Int' and 'Low'; see Methods) we observed an inverse correlation between miR-455-5p and PD-L1 expression (Fig. 6F). Lastly, we investigated miR-455-5p and PD-L1 association in a publicly available dataset of NSCLC patients after chemotherapy treatment ($N=131$, [31]; Additional file 12: Fig. S8 A-C; see also Supplementary Methods). GSEA using a curated gene set representing miR-455-5p-predicted target genes ($n=349$, Additional file 3: Data File 3; see Methods) revealed a positive enrichment (FDR < 0.05) of miR-455-5p targets in high PD-L1 chemoresistant NSCLC (Additional file 12: Fig. S8A). Notably, miR-455 gene is located within the intron of COL27A1 gene [32], thus we used COL27A1 expression as a surrogate of miR-455-5p expression as we previously showed [33]. Strikingly, we found that there was a significant negative correlation between COL72A1 and CD274 expression (Additional file 12: Fig. S8B–C) which further corroborated that a high PD-L1 expression was usually associated with a lower miR-455-5p expression in chemoresistant NSCLC. Next, we transfected NCI-H1993 and CDDP-R cells with miR-455-5p mimic and analyzed PD-L1 expression in vitro: miR-455-5p OE decreased the level of cell surface PD-L1 protein of NCI-H1993 and CDDP-R cells (Fig. 6G), while such effect was negligible in low-PD-L1 expressing parental cells (Fig. 6G). Importantly, similar results were obtained when we forced the expression of miR-455-5p in a primary LNmets cell line (i.e., the EBUS-52 cell line) established in our lab (Fig. 6G) (see Methods). To test the direct effect of miR-455-5p on PD-L1 expression regulation, we took advantage of custom-designed oligonucleotides (target site blockers; TSBs) that specifically prevent the binding of miR-455-5p to the *PD-L1* 3′-UTR. Transfection of TSBs in CDDP-R cells rescued PD-L1 loss of expression upon miR-455-5p OE (Fig. 6H). Strikingly, the rescue of PD-L1 expression upon TSB transfection resulted in the recovery of cisplatin resistance of CDDP-R/miR-455-5p OE cells (Fig. 6I), thus suggesting that miR-455-5p regulates cisplatin response in a PD-L1-dependent manner.

In cancer, PD-L1 expression is induced upon exposure to interferons produced by activated Natural Killer (NK) and T cells in the TME [34, 35]. We herein showed the enrichment of IFN-α and IFN-γ response pathways in low-expressing miR-455-5p cells and LNmets from pN2 patients (Fig. 5D–E). Thus, we asked whether miR-455-5p OE could affect IFN-mediated induction of PD-L1 expression. In line with our hypothesis, miR-455-5p OE was able to attenuate IFN-γ mediated PD-L1 upregulation both in parental and in CDDP-R cells (Fig. 6J). Since PD-L1 expression in tumor cells can be influenced by the aberrant activation of oncogenic signals, such as MYC, ALK, MEK-ERK, RAS and EGFR [36], and that miR-455-5p was reported to directly regulate the EGFR expression [37], we then investigated whether miR-455-5p could interfere with the EGF mediated PD-L1 expression. Interestingly, miR-455-5p OE was able to reduce the EGFR and PD-L1 expression independently of the EGF stimulation, both in normal bronchial epithelial cells (i.e., BEASB-2B) (Fig. 6K) and in NCI-H1975 lung cancer cells (which express high levels of PD-L1 due to presence of the L858R/T790M double activating mutations of *EGFR* [38]) (Fig. 6L). Notably, miR-455-5p was also predicted to target IRF2 (Fig. 5F), a well-known transcriptional repressor of PD-L1 expression [39, 40]. Indeed, we found that miR-455-5p overexpression strongly reduced IRF2 expression (Additional file 13: Fig. S9A, B) which suggests an additional miR-455-5p/IRF2 axis potentially functioning as a regulator of miR-455-5p/PD-L1 mechanism (Additional file 13: Fig. S9C), a possibility which warrants further investigation.

miR-455-5p overexpression decreases T cell apoptosis

The interaction of PD-L1 with its cognate receptor PD-1 inhibits the proliferation and activation of T cells [36]. Therefore, we asked ourselves whether miR-455-5p-dependent PD-L1 regulation in tumor cells may impact T cells viability. To this purpose, we took advantage

(See figure on next page.)

Fig. 5 miR-455-5p modulates the expression of genes involved in interferon response. **A** Volcano plot showing differentially expressed genes found by microarray analysis. *Left panel:* pN2 vs. pN0 (MED samples). *Central panel:* NCI-H1993 CTRL vs NCI-H1993 OE cells ($N=2$). *Right panel:* CDDP-R CTRL ($N=2$) vs CDDP-R OE cells ($N=2$). Gray dot, unchanged genes; Blue dot, downregulated genes (p value < 0.05; FC < -1.5); Red dot, upregulated genes (p value < 0.05; FC > 1.5). P value was calculated using the Limma moderated t test. **B** GSEA using miR-455-5p-predicted target genes in pN2 vs. pN0 (MED samples), H1993 CTRL vs H1993 OE or CDDP-R CTRL vs CDDP-R OE. NES, normalized enrichment score; FDR, false-discovery rate. (**C**) Circular plot showing GSEA results using the 'Hallmark gene sets' collection in pN2 vs pN0 (MED samples), H1993 CTRL vs H1993 OE and CDDP-R CTRL vs CDDP-R OE. In red, common enriched gene signatures having the same trend of regulation in all experimental conditions. **D** and **E** GSEA of (**D**) IFN-α and (**E**) IFN-γ response gene sets in pN2 vs pN0 (MED samples), H1993 CTRL vs H1993 OE and CDDP-R CTRL vs CDDP-R OE. **F** Venn diagram representing the overlap of genes between IFN-α/IFN-γ response gene sets and miR-455-5p target genes

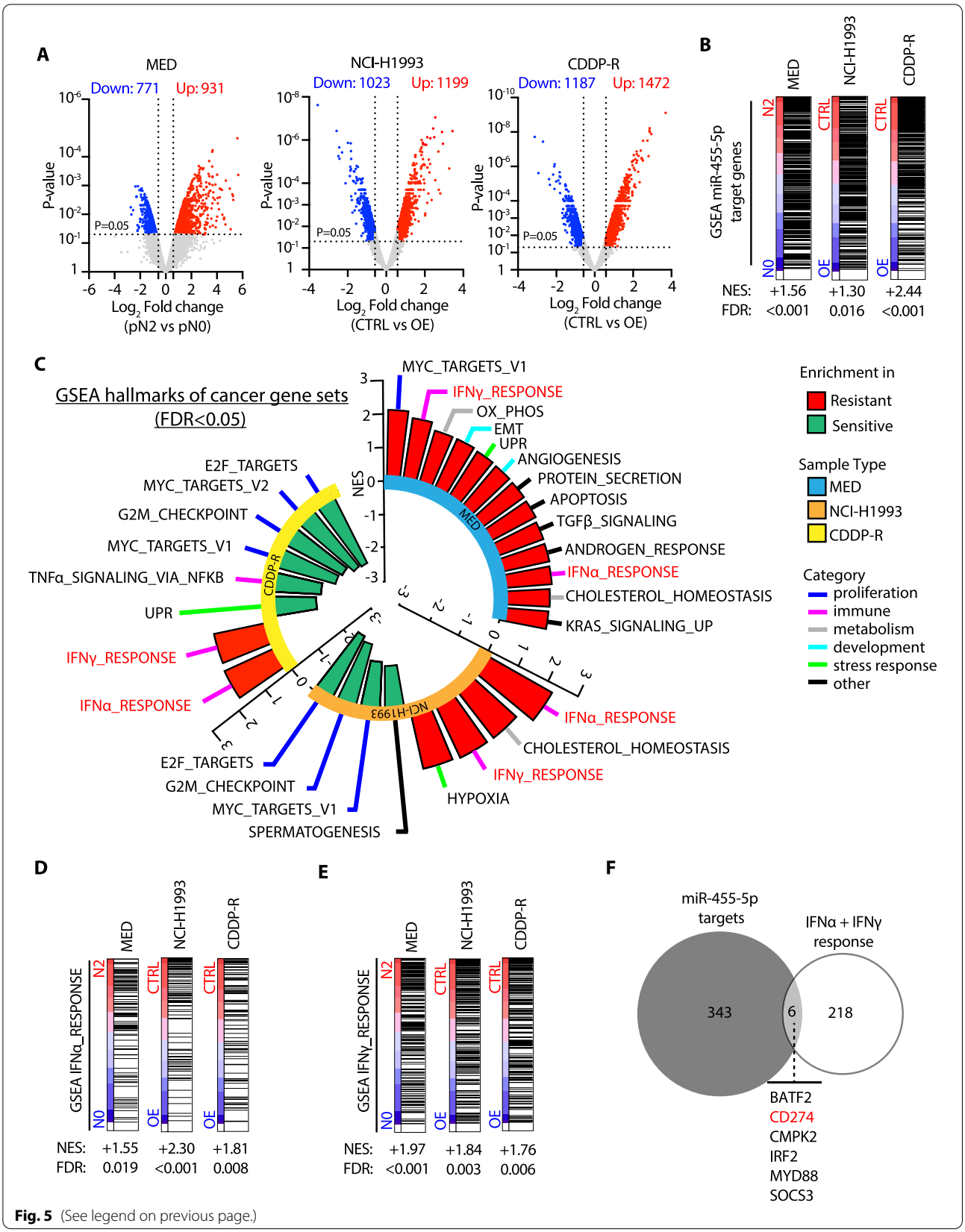

Fig. 5 (See legend on previous page.)

of Jurkat cells, a leukemic T cell line widely used in the literature for T cell signaling studies [41]. NCI-H1975 cells (miR-455-5p OE or CTRL) were co-cultured for 72 h with Jurkat cells in the presence of CD3/CD28/CD2 soluble antibody complexes to induce activation and PD-1 expression on the T cell surface (Fig. 7A). Strikingly, miR-455-5p OE decreased the percentage of apoptotic T cells when compared to T cells co-cultured with NCI-H1975 CTRL cells (Fig. 7B-C; Additional file 11: Fig. S7A). Likewise, we observed a significant reduction in apoptotic T cells when we directly silenced PD-L1 in NCI-H1975 (Fig. 7B–C; Additional file 11: Fig. S7A). Next, we analyzed the correlation of miR-455-5p expression with CD8 T cell infiltration in two independent cohorts of primary NSCLC tumors (the CSS and CIMA-CUN cohorts; Additional file 22: Table S6; Fig. 7D, E). The analysis revealed a positive correlation between miR-455-5p expression and the percentage of CD8 T cells in high tumor-infiltrating lymphocytes (TILs) tumors (Fig. 7D, E). Strikingly, when we performed a pooled analysis ($n=47$) by combining the two cohorts, we confirmed that a higher level of miR-455-5p was associated with a higher infiltration of CD8 T cells (Fig. 7F). Furthermore, we leveraged the TCGA-LUAD and TCGA-LUSC datasets to grasp further information about CD8 T cells subsets infiltration in NSCLC samples high-/low-miR-455-5p expressing: (i) TCGA samples were stratified in 'High,' 'Int' and 'Low' miR-455-5p expressing samples (see Methods); (ii) PD-L1 expression likewise expression signatures related to CD8-exhausted T cells [42] and of IFN response were analyzed in High/Int/Low miR-455-5p tumor subsets (Fig. 7G; see Methods). Strikingly, the expression levels of miR-455-5p were inversely correlated to signatures of enriched exhausted CD8 + T cell (aka GET) and of IFN response (Fig. 7G) in LUAD tumors, thus further reinforcing the link among miR-455-5p, PD-L1 and impact on T cells viability. Lastly, the analysis of the distribution of 'Immune Subtypes' introduced by Thorsson et al. [43] revealed, in LUAD low-miR-455-5p expressing samples, a depletion of the 'inflammatory subtype (C3) (enriched in proinflammatory T helper Th1 and Th17 cells) which enhances CD8 + T cells cytotoxicity (Fig. 7G). Contrariwise, the miR-455-5p expression had no effects on the immune subtypes of LUSC tumors which, by and large, showed a distinct immune composition in comparison with LUAD tumors due to the predominance of the C2 subtype and the absence of the C3 subtype (Fig. 7G). Notably, when we analyzed N2 metastasis by the CIBERSORTx algorithm [44], we found that pN2 MED samples were characterized by a trend in the reduction in cytotoxic cells, such as NK-activated cells and T cell CD8, which was in line with our previous observations (Additional file 14: Fig. S10A, Additional file 23: Table S7). Moreover, pN2 and pN0 metastases were also characterized by varying expression levels of MHC and immune-inhibitors molecules (Additional file 14: Fig. S10B).

Overall, these data suggest that miR-455-5p-dependent inhibition of PD-L1 expression may affect CD8 T cell phenotype, thus improving T cell antitumor immune response.

(See figure on next page.)

Fig. 6 miR-455-5p regulates cisplatin resistance through direct regulation of PD-L1 expression. **A** TargetScan prediction of miR-455-5p binding (seed sequence in red) to human *PD-L1* 3'UTR. **B** Spearman correlation analysis of cell surface PD-L1 expression (reciprocal of mean fluorescence intensity values) and miR-455-5p levels (Cqn) in the panel of NSCLC cell lines. **C** Bar plot of *PD-L1* expression (microarray $\log_2$ intensity) in pN2 and pN0 patients (MED samples). Error bars represent SEM. P value was calculated by Limma moderated *t* test. **D** and **E** Distribution of PD-L1 expression (TPS [tumor proportion score]) and miR-455-5p levels (Cqn) in NSCLC primary tumors obtained from CSS cohort (D) and CIMA-CUN Cohort (**E**). **F** Correlation analysis of miR-455-5p levels with PD-L1 mRNA in tumors from TGCA-LUAD and TGCA-LUSC cohorts Left: Bubble plots report the correlation coefficients. Size of the bubbles indicates statistical significance. Right: Bar plot reporting the value of miR-455-5p normalized count for each tertile threshold in TGCA-LUAD and TGCA-LUSC cohorts. The number of patients was reported inside the bar. **G** Representative flow cytometry histogram plots (left) and quantification (right) of PD-L1 median fluorescence intensity (MFI) in the indicated cell lines treated with a miR-455-5p mimic (OE) or a negative control mimic (CTRL). Results are shown as fold change of MFI relative to CTRL cells. Data are mean ± SEM ($N=4$ or 5). *P* values were calculated by one sample t test. $^{*}P<0.05$, $^{**}P<0.01$, $^{***}P<0.001$; ns, not significant. **H** Representative flow cytometry histogram plots (left) and quantification (right) of cell surface PD-L1 MFI in CDDP-R cells transfected with a miR-455-5p mimic or a negative control in the presence of a scramble TSB or a PD-L1-specific miR-455-5p TSB. Data are reported as fold change in MFI relative to CDDP-R cells transfected with a CTRL miRNA mimic and with a scramble TSB. Data are mean ± SEM ($N=6$). *P* values were calculated by one sample *t* test. $^{*}P<0.05$, $^{**}P<0.001$; ns, not significant. **I** Bar plot representing cell viability (Fold change relative to CTRL mimic in the presence of a scramble TSB) of CDDP-R cells transfected as in (**G**) and treated for 72 h with cisplatin at the indicated doses. Data are mean ± SEM ($N=5$). *P* values were calculated by one sample *t* test. $^{*}P<0.05$, $^{**}P<0.01$; ns, not significant. **J** Bar plot representing cell surface PD-L1 expression in the indicated cell lines stimulated for 48 h with ± 40 ng/ml of IFN-γ. The result is shown as fold change in the MFI relative to Parental CTRL cells. Data are mean ± SEM ($N=3$). *P* values were calculated by one sample *t* test. $^{*}P<0.05$, $^{**}P<0.01$, $^{***}P<0.001$; ns, not significant. **K** Immunoblot analysis of pEGFR, EGFR and PD-L1 in BEAS-2B transfected with a miR-455-5p mimic or a negative control and treated for 36 h with ± 40 ng/ml of EGF. GAPDH was used as loading control. **L** Immunoblot analysis of pEGFR, EGFR and PD-L1 expression in NCI-H1975 transfected with a miR-455-5p mimic or a negative control. GAPDH was used as loading control

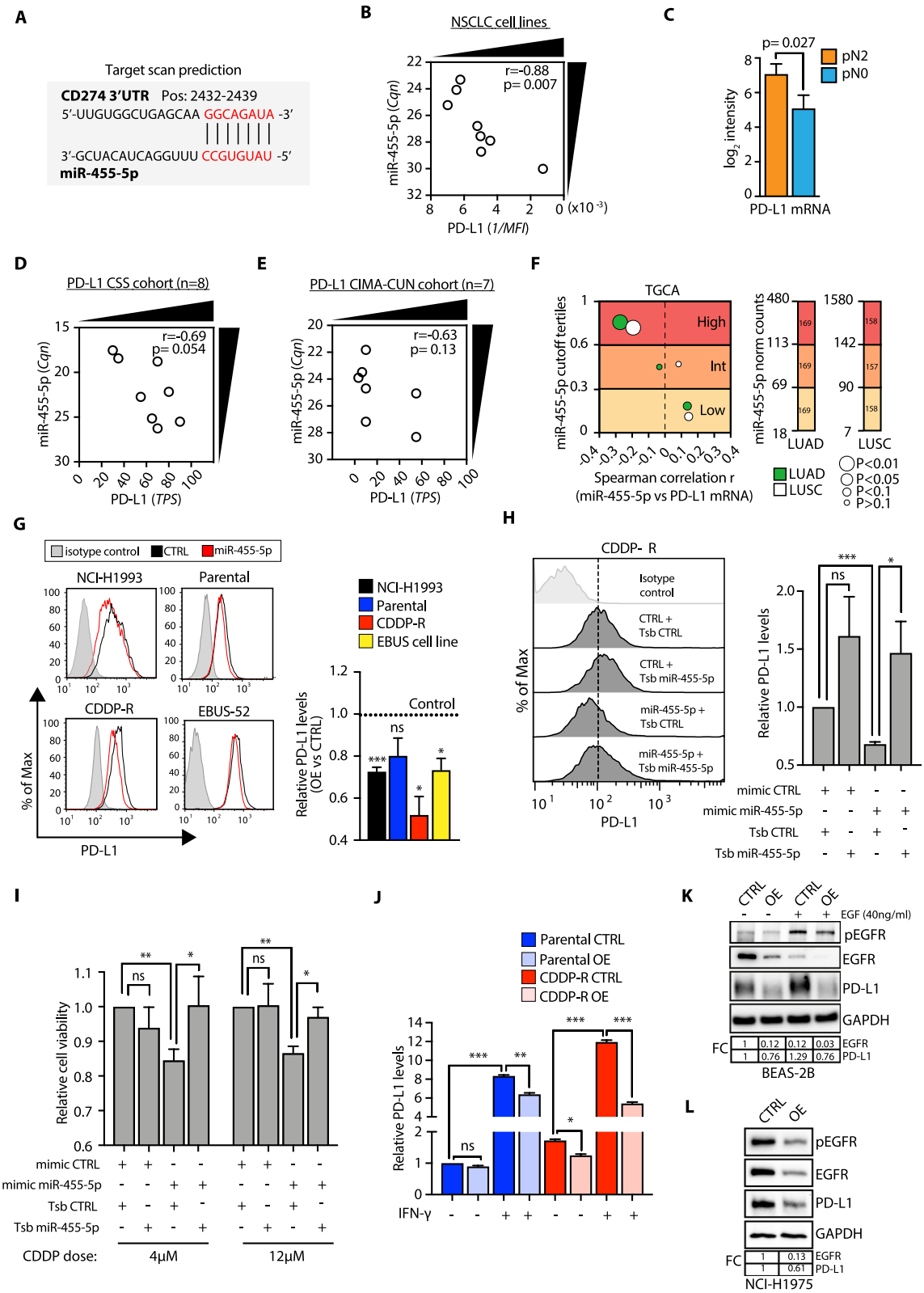

Fig. 6 (See legend on previous page.)

Discussion

Patients with locally advanced lung cancer treated by NACT in combination with surgery had better survival than patients treated by surgery alone, in randomized trials [45]. However, the response rate to NACT is still suboptimal due to the clinical and biological heterogeneity of lung tumors. Recent improvements have been made by introducing the use of ICI (e.g., nivolumab, pembrolizumab and atezolizumab [46–48]) in combination with cisplatin-based chemotherapy, to trigger the immune response against primary and metastatic lung cancer lesions [49]. Yet, the prediction of chemo/immunotherapy response as well as the identification of mechanisms of resistance in metastatic lung cancer patients is still an unmet need [50].

In recent years, microRNAs have emerged as master regulators of critical processes for lung cancer onset and progression [51]. Their role in driving lung cancer was found to be overall exerted through the expression regulation of targeted cancer-driver genes [51] and the modulation of complex cancer epigenetic mechanisms which impact tumor cells fitness by, for example, inducing EMT [52], stemness [53], immune evasion [54], and resistance to chemotherapy [55]. Furthermore, the exceptional stability of miRNA in harsh conditions and their presence in the body fluids [56] make them ideal candidates for the development of diagnostic, prognostic and predictive biomarkers [57].

Here, we performed a transcriptome analysis (miRNA and mRNA profiling) of LNmets of a cohort of patients with stage IIIA lung tumors by molecular profiling of EBUS and mediastinoscopy samples. We showed that N2 metastases resistant to NACT were characterized by an overall loss of miRNAs expression consistent with their prevalent role as tumor suppressors [58], as well as a profound reshape of the coding transcriptome. Our identified miRNA-based signatures (aka LN-signature) were accurate enough to predict NACT response which, to our knowledge, are the first of this kind and will warrant further investigations in larger and multicentric cohorts of patients.

Importantly, we unveiled that the miR-455-5p/PD-L1 axis regulates the chemotherapy response of NSCLC cells, hallmarks metastases with active IFN-γ response pathway (an inducer of PD-L1 expression [34]), and impacts T cells viability and relative abundances in TME (Fig. 7H). Remarkably, when we investigated the expression profile of miR-455-5p and correlated it with cisplatin sensitivity metrics, we found that the loss of expression of miR-455-5p hallmarked intrinsic chemoresistance of NSCLC cell lines. This was in line with the miR-455-5p regulation in EBUS and MED samples which strongly suggested the relevance of miR-455-5p in controlling mechanisms of intrinsic and acquired chemoresistance. Indeed, we showed that miR-455-5p OE was sufficient to restore cisplatin sensitivity both in vitro and in vivo.

Several mechanisms involving drug accumulation, drug efflux and mediators of response to DNA damage have been implicated in platinum resistance so far [59]. Recently, PD-L1 was shown to regulate intracellular functions of cancer cells in a cell-autonomous way besides its immune-suppressive role on the membrane, including the regulation of cisplatin resistance [29, 30]. NSCLC tumors treated with chemotherapy express higher levels of PD-L1 which, in turn, correlate with resistance and poor prognosis [26, 27, 60]. In keeping with this, we observed that PD-L1 expression is increased in resistant cells (both at basal level and upon cisplatin treatment) and direct inhibition of PD-L1 expression sensitizes cells to cisplatin treatment. Importantly, we found that miR-455-5p directly targets PD-L1 in lung

(See figure on next page.)

Fig. 7 miR-455-5p overexpression decreases T cell apoptosis. **A** Representative flow cytometry histogram plot (upper panel) and quantification (lower panel) of PD-1 MFI in Jurkat cells stimulated either with ± CD3/CD28/CD2 soluble antibody complexes for 72 h. Results are shown as fold change of MFI relative to not active cells. Data are mean ± SEM ($N = 4$). *P* value was calculated by one-sample *t* test. (**B** and **C**) NCI-H1975 cells transfected with the indicated oligos were exposed to IFN-γ for 8 h and then co-cultured for 72 h with Jurkat cells in the presence of T cell activator. **B** Representative flow cytometry histogram plots (left) and quantification (right) of PD-L1 MFI at the indicated experimental conditions. Results are shown as fold change of MFI relative to control conditions. Data are mean ± SEM ($N = 4$). *P* values were calculated by one sample *t* test. **C** Analysis of Jurkat apoptosis rate co-cultured with the indicated cell lines by Annexin V/7-AAD staining. Right panels: Representative flow cytometric plots (left) and quantification (right) of apoptotic dead Jurkat cells (Annexin V+, 7-AAD+; highlighted in red). Results are shown as fold change of apoptotic dead cells relative to matched control conditions. Data are mean ± SEM ($N = 4$). P values were calculated by one sample *t* test. **D–E–F** Distribution of the percentage of CD8+ cells and miR-455-5p expression, expressed as z-score, in NSCLC primary tumors from CD8-CIMA-CUN (D), CD8-CSS Cohort (E) and after pooling together the two cohorts (**F**). Tumors were stratified in high and low CD8 tumors based on the median value of CD8 + z-score. **G** *Left:* correlation analysis of miR-455-5p levels with PD-L1 mRNA, gene signature for exhausted CD8 + T cell (GET), IFN-γ and IFN-α response in tumors from TGCA-LUAD and TGCA-LUSC cohorts. Bubble plots reported the correlation coefficients for miR-455-5p expression with the indicated variables. The size of the bubbles indicates statistical significance calculated by the Spearman correlation analysis. Right: Bar plot reporting the Thorsson immune subtype of TGCA-LUAD and TCGA-LUSC tumors according to miR-455-5p expression. *P* value was calculated using the t test for equality of proportions (High vs Low). $^{****}P < 0.001$ (referred to C3). **H** Schematic model of the effects of miR-455-5p-dependent PD-L1 regulation in NSCLC

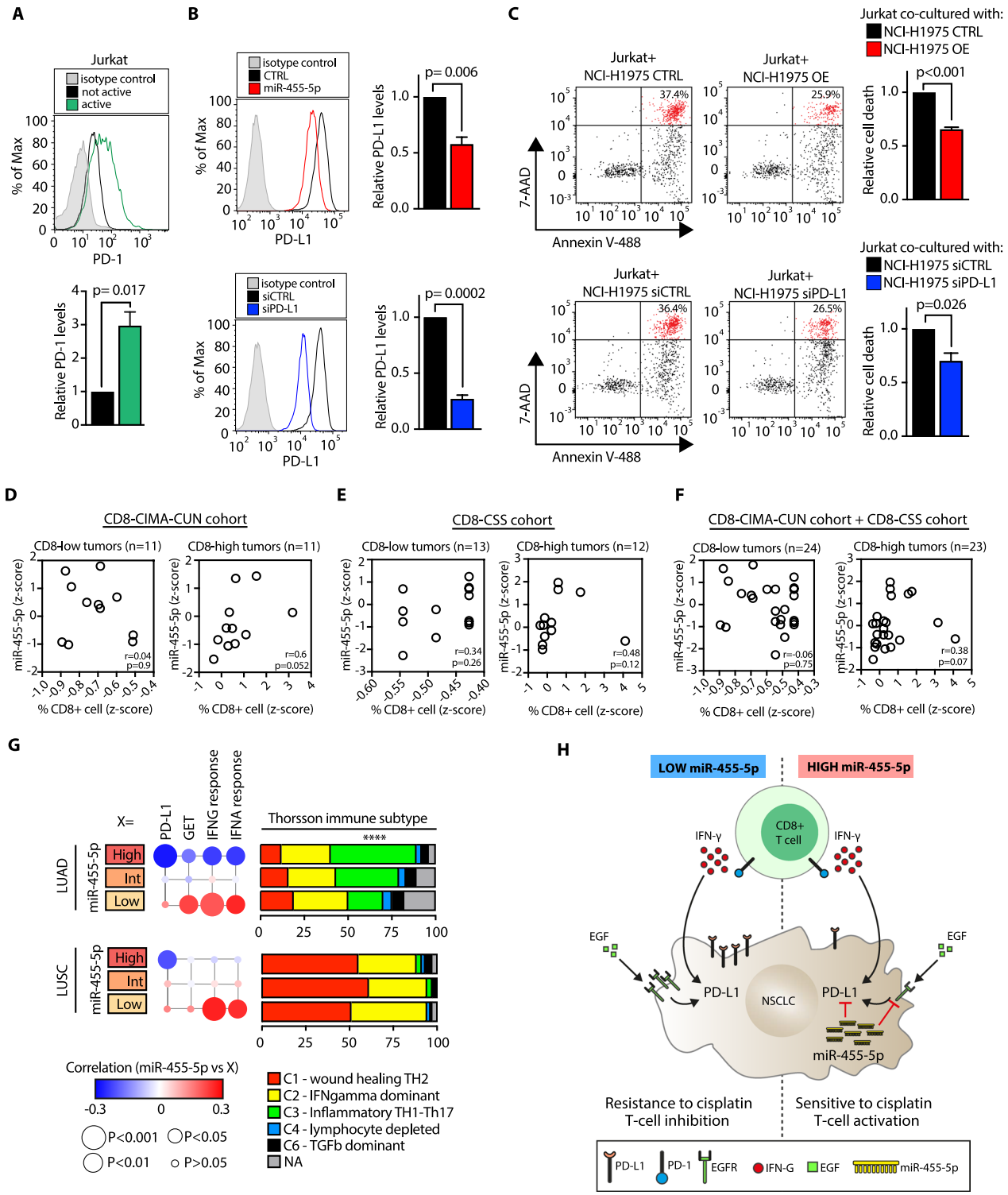

Fig. 7 (See legend on previous page.)

cancer cells and inhibits its expression thus contributing to response to cisplatin treatment. Intriguingly, other miRNAs of our LN-signature (i.e., miR-140-3p, miR-324-5p, miR-15b-5p and miR-93-5p) target PD-L1 [61] which further enforces the role of PD-L1 in NACT response in stage IIIA patients.

miR-455-5p expression has been found dysregulated in several human malignancies including colon cancer, hepatic cancer, NSCLC, gastric cancer and prostate cancer [62–65]. Recently, a work by Chen et al. has reported that miR-455-5p is able to regulate cisplatin resistance in bladder cancer via the HOXA-AS3–miR-455-5p–Notch1 axis [66]. However, in our study, neither the *HOXA-AS3* nor the *NOTCH1* expressions were found modulated upon miR-455-5p OE in vitro or in N2 metastases (Additional file 15: Fig. S11A-B). As a matter of fact, we noticed that the miR-455-5p overexpression resulted in either minor or no effect on cisplatin sensitivity in low PD-L1 expressing cells, thus highlighting the role of PD-L1 as a central mediator of the miR-455-5p activity in the context of drug resistance in NSCLC. A recent study suggested that miR-455-5p could target PD-L1 3'UTR in hepatocellular carcinoma cells [67]. However, the validation of the miRNA-binding site in the PD-L1 gene was carried out only in an unphysiological context (e.g., luciferase-based assay) and was not even confirmed in a real-world cohort of patients. Moreover, no data were presented about the role of miR-455-5p/PD-L1 axis in the regulation of cisplatin response and cancer immune evasion.

The binding of tumor PD-L1 with the receptor PD-1 on T cells activates a signaling cascade that alters the T cell activity in many ways, including the inhibition of T cell proliferation and survival, cytokine production and other effector functions [36]. Therefore, we expect that miR-455-5p-PD-L1 axis may have also a role in a non-cell-autonomous way by regulating cancer immune evasion in LNmets of stage IIIA patients. As a matter of fact, we showed that LNmets, which express low level of miR-455-5p, are characterized by a higher amount of both PD-L1 and PD-1 mRNA together with a trend of reduction in CD8 T cells, as we predicted in silico by CIBERSORTx analysis. Although an immunohistochemistry (IHC) analysis of LNmets to measure PD-L1, PD-1 and T cell markers was not feasible due to limited amount of samples, we showed in primary NSCLC tumors that a higher level of miR-455-5p was associated with decreased PD-L1 expression and increase in CD8 + T cell infiltration, in line with our hypotheses. Recently, FDA-approved neoadjuvant nivolumab plus p-doublet chemotherapy in resectable NSCLC regardless of PD-L1 tumor status [9]. Although PD-L1 expression modulation was associated with immunotherapy response [68], PD-L1 has not been considered as reliable biomarkers mainly due to its spatial and temporal heterogeneous expression [69] with PD-L1 negative tumors which responded also to ICIs [70]. However, GSEA analysis revealed that N2 metastases were enriched in a set of genes belonging to IFN-γ signature. IFN-γ is a proinflammatory cytokine produced by T cell and NK cells and is able to increase PD-L1 levels in cancer cells, thus promoting the inhibition of the T cell activity in the TME. Moreover, IFN-γ-related gene signatures have been recently reported to predict the response to anti-PD-1 therapy in melanoma [71] and NSCLC patients [72]. Interestingly, our data indicate that miR-455-5p overexpression in vitro is able to decrease both IFN-γ-mediated PD-L1 expression and the enrichment in IFN-γ related genes observed in resistant cells, which deserves further investigations to explore the role of miR-455-5p and the overall LN-signature as potential reliable biomarkers to predict the response to ICIs. Moreover, given the ability of miRNA-based LN-signature to accurately predict NACT response, such signature could also be exploited in future studies as a potential biomarker for the newly approved drug regimen based on ICIs plus NACT.

Further studies have also highlighted a high tumor heterogeneity between metastatic lesions and primary tumors in the same NSCLC patients in terms of both pathway activation and PD-L1 expression [73], which may impact chemotherapy and immunotherapy response.

Although a direct comparison between nodal metastases and primary tumors was unfeasible in our cohorts, our data represent an important step forward in understanding the molecular mechanisms driving chemoresistance in lung cancer metastatic cells. Furthermore, we provided evidence for an unedited contribution of the miR-455-5p-PD-L1 axis in the regulation of chemoresistance and immunoevasion at the level of lymph nodal metastases, thus adding new grounds for bringing chemo-immunotherapy a step closer to stage IIIA clinical practice.

Conclusions

Here, we showed that treatment naïve LNmets were characterized by distinct miRNA expression patterns which were predictive of NACT response. Importantly, by coupling whole miRNA and mRNA profiling, we unveiled a key role for the miR-455-5p/PD-L1 axis which regulates chemotherapy response and immune evasion in metastatic NSCLC cells. To our knowledge, our study represents the most comprehensive transcriptome (coding and non-coding) analysis of LNmets in NSCLC patients. In conclusion, we described novel miRNA-based biomarkers and unveiled relevant mechanisms for LNmets resistance to chemotherapy which will contribute to improving the outcome of lung cancer patients.

Methods

Tumor sample collection and processing

EBUS samples

Samples were obtained and processed as previously described [11]. EBUS-TBNA samples were collected from the mediastinal LNs station 4 and 7 of patients using a convex probe (EBUS Convex Probe BF-UC180F; Olympus), a dedicated ultrasound processor (EU-ME2; Olympus) and a 22-gauge dedicated needle (Vizishot NA-201SX-4022; Olympus). One dedicated needle passage was put into the cell culture medium for primary cell culture expansion. Briefly, EBUS-TBNA samples were centrifuged for 5 min at 1000 g at RT, resuspended in a complete medium [11] and cultured on collagen-I rat tail (Gibco) coated plates for 6 to 12 days prior to total RNA extraction (Table 1). For long-term expansion, primary cell cultures were expanded in PneumaCult Basal Ex (Stemcell Technologies). EBUS cell line used for transfection experiments was derived from LNmets of a 54 years old female with lung adenocarcinoma. Criteria for selection of patients were: i) pathologically confirmed stage IIIA-pN2 NSCLC; ii) not having been treated before for their disease; iii) suitability for NACT followed by surgery.

MED samples

Two FFPE tissue sections (5–10 µm thick) on glass slides with adequate tumor cellularity (> 60%) were selected by a certified pathologist and microdissected by scraping with a scalpel prior to RNA isolation as previously described [11] (Additional file 18: Table S2). Criteria for selection of patients were: i) pathologically confirmed stage IIIA-pN2 NSCLC; ii) not having been treated before for their disease; iii) suitability for NACT followed by surgery.

CIMA-CUN and CSS cohorts

Tumor samples were obtained from NSCLC patients who underwent surgical resection at Clínica Universidad de Navarra (Pamplona, Spain) (CUN) and at the Casa Sollievo Della Sofferenza Research Hospital (San Giovanni Rotondo, Italy) (CSS), respectively. Inclusion criteria were: (i) absence of cancer within the previous five years; (ii) complete resection of the primary tumor; (iii) no adjuvant therapy prior to surgery. Tumors were classified according to the WHO 2004 classification and the 8th TNM edition was used for tumor staging. RNA was extracted from one to two FFPE tissue sections (5 µm thick) on glass slides with adequate tumor cellularity (> 60%), selected by a pathologist. See also Additional file 21: Table S5 and Additional file 22: Table S6.

Cell lines

NCI-H2023, NCI-H1993, NCI-H1975, NCI-H838, NCI-H1944, NCI-H1437, NCI-H1573, NCI-H2126, NCI-H322M, BEAS-2B and Jurkat were obtained from ATCC and cultured in RPMI (Gibco) with 5% FBS, 1% penicillin/streptomycin except for Jurkat medium, which was supplemented with 10% FBS. Primary cell cultures from LNmets of stage IIIA NSCLC were obtained and maintained as previously described [11]. All cell lines were grown at 37 °C in a humidified incubator with 5% CO_2 and routinely tested for Mycoplasma contamination using PCR.

Creation of cisplatin-resistant cells (CDDP-R)

Cisplatin (P4394, Sigma-Aldrich) was dissolved in vehicle solution (NaCl 0.9%) at a final concentration of 1 mg/ml and stored in the dark at RT for a maximum of 28 days. NCI-H2023 cells were subjected to treatment cycles ($n = 11$), consisting of 3–4 days of cisplatin treatment and 1–2 weeks of culture in RPMI 5% FBS 1% penicillin/streptomycin to allow survived cells (i.e., the CDDP-R) to proliferate. The dose at the first treatment cycle was 0.6 µM and then increased in subsequent cycles until reaching a maximum dose of 10 µM. Parental cells treated with vehicle solution were cultured in parallel and used as a control.

Cell viability assay

Cells were seeded in 96-well plates in triplicate in 90 µL of complete media. On day 1 post-seeding, cells were treated with increasing doses of cisplatin (threefold serial dilution), or vehicle solution as a control. Cell viability was assessed by adding CyQUANT Cell Proliferation Assay Kit (Life Technologies) in a ratio of 1:10 directly in complete media. Fluorescence was measured at 480/528 nm using a Sinergy HT (Biotek) microplate reader and IC_{50} was estimated using the online tool GR calculator [74].

Cell transfection experiments

All transfection experiments were carried out by performing reverse transfection with Lipofectamine RNAiMAX (Thermo Fisher Scientific) according to the manufacturer's instructions. The following oligos at the indicated concentration were used: 5 nM of miR-455-5p mimic (MSY0003150, Qiagen) or recommended All Stars negative control siRNA (cat. 1027281, Qiagen); 7.5 nM of PD-L1-specific miR-455-5p TSB (339194; sequence: GTA GACTATGTGCCTTTGCTCAG; Qiagen) or scramble TSB (339194; sequence: ACGTCTATACGCCCA; Qiagen); 10 nM of siRNA against *CD274* (HSS120932, Thermo Fisher scientific) or recommended Stealth RNAi

negative control Med GC (12935-300, Thermo Fisher scientific).

Jurkat T cell apoptosis assay

Transfected NCI-H1975 were seeded overnight to allow them to adhere to culture plates. The day after, tumor cells were stimulated with 40 ng/ml of IFN-γ for 8 h and then co-cultured with Jurkat cells in the presence of ImmunoCult human CD3/CD28/CD2 T cell activator (Stemcell Technologies) at Jurkat cells to NCI-H1975 ratio of 1:4. After 72 h, Jurkat cells were recovered from the co-culture and analyzed by AnnexinV-488 (Thermo Fisher) and 7-AAD (BD Pharmingen) staining in a BD FACS CANTO Cytometer. The gating strategy used to analyze apoptosis is reported in Additional file 11: Fig. S7.

Total RNA (including small RNA) isolation

Total RNA from commercial cell lines, EBUS samples and MED samples was isolated using, respectively, miRNeasy kit, AllPrep DNA/RNA/miRNA Universal Kit and AllPrep DNA/RNA FFPE Kit, respectively, according to the with manufacturer's instructions. Total RNA quantification was carried out using the NanoDrop® ND-1000 spectrophotometer or Qubit RNA HS Assay Kit (Invitrogen).

Quantitative real time-PCR (qRT-PCR) of miRNAs and mRNAs

For qRT-PCR of miRNAs, 10 ng of total RNA was reverse-transcribed using a TaqMan MicroRNA Reverse Transcription Kit (Thermo Fisher Scientific) and RT-specific primers for miRNAs (Thermo Fisher Scientific, See Additional file 25: Table S9). 2.5 µL of RT product was pre-amplified for 14 cycles using the TaqMan PreAMP Master Mix and miRNA Taqman assay (see Additional file 25: Table S9). The expression levels of miRNAs were normalized to the housekeeping gene U6 snRNA. For qRT-PCR of transcripts of commercially available cell lines, 1 µg of total RNA was reverse-transcribed using a High Capacity cDNA Reverse Transcription Kit (Thermo Fisher Scientific) according to manufacturer instructions. For qRT-PCR of transcripts of EBUS and MED samples, 200 ng of total RNA was reverse-transcribed with the SuperScript VILO cDNA Synthesis Kit (Thermo Fisher Scientific) in 20 µL of final volume and then cDNA was pre-amplified for 10 cycles. cDNA was amplified with the TaqMan Gene Expression assay (Thermo Fisher Scientific, See Additional file 25: Table S9) and QuantStudio 12 k Flex thermocycler (Thermo Fisher Scientific) using the manufacturer's recommended cycling conditions. Data were normalized using the geometric mean of three genes (ESD1, GUSB and HPRT) as reference. Data normalization for both miRNAs and mRNAs was performed by using the delta–delta CT method or the calculation of the normalized Cq as previously described [75].

Whole miRNA expression profile

Ten nanograms of total RNA was reverse-transcribed with MegaplexTM miRNA-specific stem-loop RT Primers Human Pool A v 2.1 (Thermo Fisher Scientific) and TaqMan® MicroRNA reverse transcription kit (Thermo Fisher Scientific) according to the manufacturer's instructions. Five microliters of reverse-transcribed product was pre-amplified for 14 cycles using the TaqMan PreAMP Master Mix and Megaplex PreAMP primers Pool A v 2.1 according to the manufacturer's instructions (Thermo Fisher Scientific). The PCR reaction was performed using the TaqMan Universal Master Mix II, No AmpErase UNG (Thermo Fisher Scientific) by loading 100 µL of the pre-amplified mixture (final dilution 1:200) in each of the eight lanes of the TaqMan® Low Density Array miRNA Panel A v 2.0 (Thermo Fisher Scientific). Real-Time PCR was carried out on the QuantStudio 12 k (Thermo Fisher Scientific) according to the manufacturer's cycling conditions and by setting an automatic threshold. Cq data of miRNAs were normalized (Cqn) using U6 snRNA as previously described [75]. miRNAs with a $Cq < 30.01$ in at least 50% of samples among one of the experimental groups tested in the analysis were considered as detected.

Zebrafish cell-derived xenograft (zCDX)

zCDX models were developed by a CRO (BioReperia AB). Transgenic Tg(fli1:EGFP)y1 zebrafish embryos were raised at 28 °C for 48 h in E3 embryo medium (containing per liter: 0.286 g NaCl, 0.048 g CaCl2, 0.081 g MgSO4 and 0.0126 g KCl with 0.2 mM 1-Phenyl-2-Thiourea aka PTU). At 2 days post-fertilization, embryos were injected subcutaneously in the perivitelline space with transfected parental and CDDP-R cells previously labeled with FAST Dil™ oil (Thermo Fisher Scientific) and treated with ± Cisplatin 5 mg/L for 3 days. Images of tumors were taken by using a fluorescent stereoscope with a K5 camera (Leica) and LAS X software v3.7.1.21655 at 100× magnification with no binning. Images of tumors were taken right after injection (day 1) and after drug treatment (day 4). Images were automatically analyzed by using the HuginMunin software v2.7.0.0 (BioReperia AB). Tumor growth regression was calculated by dividing the number of tumor pixels on day 4 by the number of tumor pixels on day 1 in the same embryo and multiplied by 100.

Genome-wide expression profiling

Gene expression profiling of MED samples and NSCLC cell lines (two independent biological replicates) was carried out using the GeneChip® Pico reagent Kit and the GeneChip® WT Plus reagent Kit, respectively. For both reagents, the GeneChip® Human Clarion S Array (Thermo Fisher Scientific) was used according to the manufacturer's instructions. Quality control, normalization of CEL files and statistical analysis were performed using the Transcriptome Analysis Console (TAC) software v4.0 (Thermo Fisher Scientific) by performing the 'Gene level SST-RMA' summarization method with human genome version hg38. Differentially expressed genes were defined as those with a fold change (FC) difference of at least 1.5 and a p value less than 0.05. For MED samples, 5 pN2 and 5 pN0 samples balanced for age, sex and histotype were pooled to obtain 2 pools for each experimental condition (pN2 and pN0). Microarray expression data can be found in the GEO database (GSE193707).

Predictive risk model

A ridge-penalized unconditional logistic regression was applied in the training set to model the odds of responding as a function of the 16 miRNAs that were scored as differentially expressed between responder and non-responder patients in the EBUS samples (16-miRNA model). The same strategy was used for the 14-miRNA and 4-miRNA models. Cross-validated (tenfold) log-likelihood with optimization (50 simulations) of the tuning penalty parameter was applied. The probability of being a responder was estimated, and model performance was assessed using the area under the receiver operating curve (AUC). Min–max scaling of miRNAs expression in the validation set was implemented before applying the predictive model. LASSO approach was used to reduce the number of predictors.

Analysis of cell line publicly available datasets

Cell viability of cisplatin for the indicated dataset was downloaded directly from the DepMap portal (https://depmap.org/portal/compound/cisplatin?tab=dose-curves). Analysis of cell viability data was restricted only to NSCLC cell lines for which miRNA expression data was available in the CCLE dataset. Median cell viability was calculated at each concentration and plotted. Quality control (QC) for IC_{50} estimation was applied following instructions reported in Sebaugh et al. [76]. Briefly, we estimate IC_{50} values for cell lines in each dataset by taking advantage of cell viability data downloaded from DepMap portal and the online software 'GR calculator.' QC criteria applied were: at least two concentrations below the 50% response concentration and above the 50% response. Only proportions of cell lines in each dataset for which IC_{50} estimation was accurate according to Sebaugh et al. were reported (see Additional file 18: Table S2).

CIBERSORTx analysis

CIBERSORTx [44] was run using the online Web tool (https://cibersortx.stanford.edu) and following the developers' instructions. The CIBERSORTx analysis was conducted using the following settings: LM 22 as signature matrix file, absolute mode running and 100 permutations. CIBERSORTx score is an estimation of cell fraction of each specific subpopulation in each tumor sample. CIBERSORTx complete results were reported in Additional file 23: Table S7.

Gene set enrichment analysis (GSEA)

GSEA (GSEA, https://www.gsea-msigdb.org/gsea/index.jsp) was performed using Signal2Noise metric, 1000 random sample sets permutation, and median gene expression values for class comparison. For enrichment analysis of hallmarks of cancer, we used the gene matrix h.all.v7.4 symbols.gmt available from MSigDB. For miR-455-5p target enrichment analysis, we built a custom gene matrix by including human genes that were highly or moderately predicted to be miR-455-5p targets (cumulative weighted context + + score ≤ -0.2) by TargetScan (release 7.2) and were well expressed ($\log_2$ intensity > 4) in all samples used in each analysis. Significant gene sets were considered as those with a false-discovery rate (q value) of less than 5%. For single-sample gene set enrichment analysis of TGCA cohorts, ssGSEA scores were calculated by using the GSVA package in R. Gene signatures for exhausted CD8 + T cell were obtained from Cai et al. [42], while gene signatures for IFN-γ and IFN-α response were downloaded from MSigDB hallmark gene sets (version h.all.v7.4 symbols.gmt).

Statistics

Hierarchical clustering was performed using Cluster 3.0 (C Clustering Library 1.56; http://bonsai.hgc.jp/~mdehoon/software/cluster/software.htm) and Java Tree View (Version 1.1.6r4; http://jtreeview.sourceforge.net). The uncentered correlation and centroid linkage clustering method was used. Heatmaps were obtained by using MORPHEUS (https://software.broadinstitute.org/morpheus/) or Java Tree View. All graphs and statistical analyses were performed using Prism (version 7.0e), SPSS (version 15.0), SAS software and R 3.3.1 (R Core Team, 2016). The normality of data was controlled by Shapiro–Wilk and D'Agostino & Pearson normality tests. The details about statistical tests, number of independent replicates (N)

and definition of error bars were specified in the figure legends. Statistical output (p value) was represented by asterisks as follows: nonsignificant (ns) > 0.05, $^{*}p \leq 0.05$, $^{**}p \leq 0.01$, $^{***}p \leq 0.001$, $^{****}p \leq 0.0001$. A $p < 0.05$ was considered to be statistically significant. The sample size for tissue-based assays was chosen on the basis of sample availability. The investigators were not blinded when analyzing the data except for IHC analysis and zebrafish experiments.

Abbreviations

3′-UTR: 3′ Untranslated region; ACTA-2: Actin alpha 2, smooth muscle; AUC: Area under the curve; CC10: Clara cell 10; CCLE: Cancer Cell Line Encyclopedia; CD90: Cluster of differentiation 90; CDDP: Cisplatin; CDH5: Cadherin 5; CTRL: Control; CTRPv2: Cancer Therapeutics Response Portal; DMSO: Dimethyl sulfoxide; E-CAD: E-cadherin; EBUS-TBNA: Endobronchial ultrasound transbronchial needle aspiration; EGFR: Epidermal growth factor receptor; EMT: Epithelial-to-mesenchymal transition; ESD1: Esterase D; FDR: False discovery rate; FFPE: Formalin-fixed paraffin-embedded; GAPDH: Glyceraldehyde-3-phosphate dehydrogenase; GDSC1-2: Genomics of Drug Sensitivity in Cancer; GET: Gene signature of exhausted CD8 + T cell; GSEA: Gene set enrichment analysis; HPRT1: Hypoxanthine phosphoribosyltransferase 1; ICI: Immune checkpoint inhibitors; IFN-α: Interferon-alpha; IFN-γ: Interferon-gamma; IHC: Immunohistochemistry; KRT5: Keratin 5; LN: Lymph node; LNmets: Lymph nodal metastases; LUAD: Lung adenocarcinoma; LUSC: Lung squamous cell carcinoma; MED: Mediastinoscopy; N-CAD: N-cadherin; NACT: Neoadjuvant chemotherapy; NES: Normalized enriched score; NK: Natural killer; NKX2-1: NK2 Homeobox 1; NSCLC: Non-small cell lung cancer; OE: Overexpression; P-doublet: Platinum-based doublet; Pan-CK: Pan-cytokeratin; PRISM: Profiling relative inhibition simultaneously in mixtures; PTPRC: Protein tyrosine phosphatase receptor type C; SFTPC: Surfactant protein C; SLUG: Zinc finger protein SNAI2; SOX2: SRY-box transcription factor 2; TILs: Tumor-infiltrating lymphocytes; TLDA: TaqMan low-density array; TME: Tumor microenvironment; TSB: Target site blockers; TWIST1: Twist family BHLH transcription factor 1; VIM: Vimentin; zCDX: Zebrafish cell-derived xenograft; ZEB1: Zinc finger E-box binding homeobox 1.

Supplementary Information

The online version contains supplementary material available at https://doi.org/10.1186/s13045-022-01394-1.

Additional file 1. **Data File S1**. Expression data of the 377 miRNA analysed in EBUS cohort.

Additional file 2. **Data File S2**. Expression data of the 377 miRNA analysed in MED cohort.

Additional file 3. **Data File S3**. miR-455-5p GSEA custom gene matrix.

Additional file 4. **Data File S4**. Western blot quantification.

Additional file 5. **Figure S1**. Whole miRNA expression profile of chemo-naïve metastatic tissue from stage III NSCLC patients.

Additional file 6. **Figure S2**. Biological characterization of Cisplatin resistant cells.

Additional file 7. **Figure S3**. Implantation analysis of CDX in zebrafish.

Additional file 8. **Figure S4**. miR-455-5p overexpression decreases the proliferation rate of NSCLC cells.

Additional file 9. **Figure S5**. Higher basal levels of PD-L1 are associated to cisplatin resistance in NSCLC in vitro.

Additional file 10. **Figure S6**. PD-L1 expression contributes to cisplatin resistance in an in vitro model of acquired resistance.

Additional file 11. **Figure S7**. Gating strategy used to analyze Jurkat T cells apoptosis after co-culture with NCIH1975 tumor cells.

Additional file 12. **Figure S8**. Analysis of miR-455-5p and PD-L1 association in post-chemotherapy samples of NSCLC patients.

Additional file 13. **Figure S9**. miR-455-5p regulates IRF2 expression in NSCLC cell lines.

Additional file 14. **Figure S10**. Estimation of immune features of chemo-naïve lung metastatic tumor tissue.

Additional file 15. **Figure S11**. miR-455-5p is not involved in the regulation of NOTCH-1 and HOXA-AS3 expression in NSCLC.

Additional file 16. Supplemental Material.

Additional file 17. **Table S1**. Predictive models (miRNA) characteristics.

Additional file 18. **Table S2**. Quality control of IC50 estimation from publicy available dataset

Additional file 19. **Table S3**. GSEA of hallmark of cancer signatures of transcriptomic data

Additional file 20. **Table S4**. Clinical-pathological features of TGCA-LUAD and TGCA-LUSC cohorts.

Additional file 21. **Table S5**. Clinical-pathological features of PD-L1 CSS (A) and CIMA-CUN (B) cohort.

Additional file 22. **Table S6**. Clinical-pathological features of CD8 CIMA-CUN (A) and CD8 CSS (B) cohort.

Additional file 23. **Table S7**. Immune cell estimation of MED samples by CIBERSORTx.

Additional file 24. **Table S8**. Primary and secondary antibody used for western blot, immunofluorescence and flow cytometry.

Additional file 25. **Table S9**. Primer used for qRT-PCR.

Acknowledgements

We thank Dr. Lucia Anna Muscarella and Dr. Vincenzo Giambra (Fondazione IRCCS Casa Sollievo della Sofferenza; San Giovanni Rotondo, Italy) for sharing NCI-H1573, NCI-H2126, NCI-H1975 and Jurkat cells, respectively. We thank Dr. Karmele Valencia for her help in performing the IHC analysis of the CIMA-CUN cohort and Dr. Rose Mary Carletti for technical support with TLDA qRT-PCR experiments. We thank Dr. Miriam Kuku Afanga for technical support with immunoblot experiments. Dr. Fabrizio Bianchi wishes to thank Prof. Pier Paolo di Fiore (European Institute of Oncology) for his support and mentorship. We are grateful to Chiara Di Giorgio for English editing and manuscript proofreading.

Author contributions

R.C. and F.B. contributed to conceptualization. R.C., T.C., E.D., V.M., O.P., E.B., F.M., M.B., P.G., L.M., C.C., J.G., L.S., J.S., A.P., and F.B. contributed to methodology. R.C., T.C., E.D., M.C., F.M.Z., L.M., J.G., L.S., and F.B. investigated the study. R.C., T.C., E.D., V.M., L.M., and F.B. visualized the study. F.B. performed funding acquisition and project administration. R.C. and F.B. contributed to supervision, writing—original draft, and writing—review and editing. All authors read and approved the final manuscript.

Funding

The research leading to these results has received funding from AIRC under IG 2019—ID. 22827 project—P.I. Bianchi Fabrizio, from AIRC under MFAG-17568—P.I. Bianchi Fabrizio; this study was also supported in part by the Italian Ministry of Health [GR-2016–02363975 and CLEARLY to F.B.; GR-2019-12370460 to T.C.]. R.C. was a recipient of a fellowship from Fondazione Umberto Veronesi and of a fellowship from Fondazione Pezcoller. T.C. was a recipient of a fellowship from Associazione Italiana Ricerca sul Cancro (#19548) and of a fellowship from Fondazione Umberto Veronesi. L.M.M. was supported by FIMA, Fundación ARECES and ISCIII-Fondo de Investigación Sanitaria-Fondo Europeo de Desarrollo Regional (PI19/00098). The study funders had no role in the design of the study, the collection, analysis, and interpretation of the data, the writing of the manuscript, and the decision to submit the manuscript for publication. All authors gave their consent to publication.

Availability of data and materials
All data generated or analyzed during this study are included in this published article and its supplementary information files. The datasets generated during the current study (microarray expression data) are available in the GEO database (GSE193707). The Web link to public datasets analyzed during the current study is available in the materials section.

Declarations

Ethics approval and consent to participate
The institutional ethical committees approved this study (registration number: R65/14-IEO76; BIO-EBUS-V1.0_Ott19; BIO-POLMONE-V1.0_Giu16), and informed consent was obtained from all patients enrolled.

Consent for publication
Not applicable.

Competing interests
The authors declare that they have no competing interests.

Author details
[1]Unit of Cancer Biomarkers, Fondazione IRCCS Casa Sollievo della Sofferenza, Viale Padre Pio 7, 71013 San Giovanni Rotondo, FG, Italy. [2]Division of Thoracic Surgery, IEO, European Institute of Oncology IRCCS, 20141 Milan, Italy. [3]Division of Medical Genetics, Fondazione IRCCS Casa Sollievo della Sofferenza, Viale Cappuccini Snc, 71013 San Giovanni Rotondo, FG, Italy. [4]Clinical Genomics Unit, European Institute of Oncology, Milan, Italy. [5]Department of Experimental Oncology, European Institute of Oncology, Milan, Italy. [6]European Institute of Oncology IRCCS, Milan, Italy. [7]IFOM, Fondazione Istituto FIRC di Oncologia Molecolare, Via Adamello 16, 20139 Milan, Italy. [8]Division of Pathology, European Institute of Oncology IRCCS, 20141 Milan, Italy. [9]Unit of Pathology, Fondazione IRCCS Casa Sollievo della Sofferenza, Viale Cappuccini Snc, 71013 San Giovanni Rotondo, FG, Italy. [10]Solid Tumors Program, Center of Applied Medical Research (CIMA), University of Navarra and IDISNA, Pamplona, Spain. [11]Department of Pathology, Clínica Universidad de Navarra, Madrid, Spain. [12]CIBERONC, Madrid, Spain. [13]Pneumology Unit, Department of Medical Sciences, Fondazione IRCCS Casa Sollievo della Sofferenza, 71013 San Giovanni Rotondo, FG, Italy. [14]Department of Oncology and Hemato-Oncology, University of Milan, Milan, Italy. [15]Present Address: Non-Coding RNAs and RNA-Based Therapeutics, Istituto Italiano Di Tecnologia, CMP3VdA, Via Lavoratori Vittime del Col du Mont 28, 11100 Aosta, Italy.

Received: 10 May 2022 Accepted: 19 December 2022
Published online: 31 December 2022

References

1. Siegel RL, Miller KD, Fuchs HE, Jemal A. Cancer statistics, 2021. CA A Cancer J Clin. 2021;71:7–33.
2. Goldstraw P, Chansky K, Crowley J, Rami-Porta R, Asamura H, Eberhardt WEE, et al. The IASLC Lung Cancer Staging Project: proposals for revision of the TNM stage groupings in the forthcoming (Eighth) edition of the TNM classification for lung cancer. J Thorac Oncol. 2016;11:39–51.
3. NSCLC Meta-analysis Collaborative Group. Preoperative chemotherapy for non-small-cell lung cancer: a systematic review and meta-analysis of individual participant data. Lancet. 2014;383:1561–71.
4. Hellmann MD, Chaft JE, William WN, Rusch V, Pisters KMW, Kalhor N, et al. Pathological response after neoadjuvant chemotherapy in resectable non-small-cell lung cancers: proposal for the use of major pathological response as a surrogate endpoint. Lancet Oncol. 2014;15:e42-50.
5. Betticher DC, Hsu Schmitz SF, Totsch M, Hansen E, Joss C, von Briel C, et al. Mediastinal lymph node clearance after docetaxel-cisplatin neoadjuvant chemotherapy is prognostic of survival in patients with stage IIIA pN2 non-small-cell lung cancer: a multicenter phase II trial. J Clin Oncol. 2003;21:1752–9.
6. Spaggiari L, Casiraghi M, Guarize J, Brambilla D, Petrella F, Maisonneuve P, et al. Outcome of Patients With pN2 "Potentially Resectable" Nonsmall Cell Lung Cancer Who Underwent Surgery After Induction Chemotherapy. Semin Thorac Cardiovasc Surg. 2016;28:593–602.
7. de Bruin EC, McGranahan N, Mitter R, Salm M, Wedge DC, Yates L, et al. Spatial and temporal diversity in genomic instability processes defines lung cancer evolution. Science. 2014;346:251–6.
8. Zhang J, Fujimoto J, Wedge DC, Song X, Seth S, Chow CW, et al. Intratumor heterogeneity in localized lung adenocarcinomas delineated by multiregion sequencing. Science. 2014;346:256–9.
9. Forde PM, Spicer J, Lu S, Provencio M, Mitsudomi T, Awad MM, et al. Neoadjuvant nivolumab plus chemotherapy in resectable lung cancer. N Engl J Med. 2022;386:1973–85.
10. Calvo V, Sierra-Rodero B, Cruz-Bermúdez A, Provencio M. Role of immunotherapy in stage IIIA non-small cell lung cancer: a narrative review. Curr Chall Thorac Surg. 2021;3:38–38.
11. Guarize J, Bianchi F, Marino E, Belloni E, Vecchi M, Donghi S, et al. MicroRNA expression profile in primary lung cancer cells lines obtained by endobronchial ultrasound transbronchial needle aspiration. J Thorac Dis. 2018;10:408–15.
12. Rees MG, Seashore-Ludlow B, Cheah JH, Adams DJ, Price EV, Gill S, et al. Correlating chemical sensitivity and basal gene expression reveals mechanism of action. Nat Chem Biol. 2016;12:109–16.
13. Seashore-Ludlow B, Rees MG, Cheah JH, Cokol M, Price EV, Coletti ME, et al. Harnessing connectivity in a large-scale small-molecule sensitivity dataset. Cancer Discov. 2015;5:1210–23.
14. Basu A, Bodycombe NE, Cheah JH, Price EV, Liu K, Schaefer GI, et al. An interactive resource to identify cancer genetic and lineage dependencies targeted by small molecules. Cell. 2013;154:1151–61.
15. Yang W, Soares J, Greninger P, Edelman EJ, Lightfoot H, Forbes S, et al. Genomics of drug sensitivity in cancer (GDSC): a resource for therapeutic biomarker discovery in cancer cells. Nucleic Acids Res. 2013;41:D955-961.
16. Corsello SM, Nagari RT, Spangler RD, Rossen J, Kocak M, Bryan JG, et al. Discovering the anticancer potential of non-oncology drugs by systematic viability profiling. Nat Cancer. 2020;1:235–48.
17. Hall MD, Telma KA, Chang K-E, Lee TD, Madigan JP, Lloyd JR, et al. Say No to DMSO: dimethylsulfoxide inactivates cisplatin, carboplatin, and other platinum complexes. Cancer Res. 2014;74:3913–22.
18. van Moorsel CJA, Kroep JR, Pinedo HM, Veerman G, Voorn DA, Postmus PE, et al. Pharmacokinetic schedule finding study of the combination of gemcitabine and cisplatin in patients with solid tumors. Ann Oncol. 1999;10:441–8.
19. Kuenen BC, Rosen L, Smit EF, Parson MRN, Levi M, Ruijter R, et al. Dose-finding and pharmacokinetic study of cisplatin, gemcitabine, and SU5416 in patients with solid tumors. JCO. 2002;20:1657–67.
20. Lin Z, Pan J, Chen L, Wang X, Chen Y. MiR-140 resensitizes cisplatin-resistant NSCLC cells to cisplatin treatment through the SIRT1/ROS/JNK pathway. OTT. 2020;13:8149–60.
21. Wu S, Wang H, Pan Y, Yang X, Wu D. miR-140-3p enhances cisplatin sensitivity and attenuates stem cell-like properties through repressing Wnt/β-catenin signaling in lung adenocarcinoma cells. Exp Ther Med. 2020;20:1664–74.
22. Shibue T, Weinberg RA. EMT, CSCs, and drug resistance: the mechanistic link and clinical implications. Nat Rev Clin Oncol. 2017;14:611–29.
23. Fazio M, Ablain J, Chuan Y, Langenau DM, Zon LI. Zebrafish patient avatars in cancer biology and precision cancer therapy. Nat Rev Cancer. 2020;20:263–73.
24. Xiao J, Glasgow E, Agarwal S. Zebrafish Xenografts for drug discovery and personalized medicine. Trends Cancer. 2020;6:569–79.
25. Agarwal V, Bell GW, Nam JW, Bartel DP. Predicting effective microRNA target sites in mammalian mRNAs. eLife. 2015;4.
26. Parra ER, Villalobos P, Behrens C, Jiang M, Pataer A, Swisher SG, et al. Effect of neoadjuvant chemotherapy on the immune microenvironment in non–small cell lung carcinomas as determined by multiplex immunofluorescence and image analysis approaches. J Immunotherapy Cancer. 2018;6:48.
27. Zhang P, Ma Y, Lv C, Huang M, Li M, Dong B, et al. Upregulation of programmed cell death ligand 1 promotes resistance response in non-small-cell lung cancer patients treated with neo-adjuvant chemotherapy. Cancer Sci. 2016;107:1563–71.
28. Shin J, Chung J-H, Kim SH, Lee KS, Suh KJ, Lee JY, et al. Effect of platinum-based chemotherapy on PD-L1 expression on tumor cells in non-small cell lung cancer. Cancer Res Treat. 2019;51:1086–97.
29. Tu X, Qin B, Zhang Y, Zhang C, Kahila M, Nowsheen S, et al. PD-L1 (B7–H1) competes with the RNA exosome to regulate the DNA damage response

and can be targeted to sensitize to radiation or chemotherapy. Mol Cell. 2019;74:1215–26.
30. De S, Holvey-Bates EG, Mahen K, Willard B, Stark GR. The ubiquitin E3 ligase FBXO22 degrades PD-L1 and sensitizes cancer cells to DNA damage. Proc Natl Acad Sci USA. 2021;118:e2112674118.
31. Byers LA, Diao L, Wang J, Saintigny P, Girard L, Peyton M, et al. An epithelial-mesenchymal transition gene signature predicts resistance to EGFR and PI3K inhibitors and identifies Axl as a therapeutic target for overcoming EGFR inhibitor resistance. Clin Cancer Res. 2013;19:279–90.
32. La T, Liu GZ, Farrelly M, Cole N, Feng YC, Zhang YY, et al. A p53-responsive miRNA network promotes cancer cell quiescence. Cancer Res. 2018;78:6666–79.
33. Monterisi S, D'Ario G, Dama E, Rotmensz N, Confalonieri S, Tordonato C, et al. Mining cancer gene expression databases for latent information on intronic microRNAs. Mol Oncol. 2015;9:473–87.
34. Garcia-Diaz A, Shin DS, Moreno BH, Saco J, Escuin-Ordinas H, Rodriguez GA, et al. Interferon receptor signaling pathways regulating PD-L1 and PD-L2 expression. Cell Rep. 2017;19:1189–201.
35. Yi M, Niu M, Xu L, Luo S, Wu K. Regulation of PD-L1 expression in the tumor microenvironment. J Hematol Oncol. 2021;14:10.
36. Sun C, Mezzadra R, Schumacher TN. Regulation and function of the PD-L1 checkpoint. Immunity. 2018;48:434–52.
37. Ning T, Peng Z, Li S, Qu Y, Zhang H, Duan J, et al. miR-455 inhibits cell proliferation and migration via negative regulation of EGFR in human gastric cancer. Oncol Rep. 2017;38:175–82.
38. Peng S, Wang R, Zhang X, Ma Y, Zhong L, Li K, et al. EGFR-TKI resistance promotes immune escape in lung cancer via increased PD-L1 expression. Mol Cancer. 2019;18:165.
39. Wu A, Wu Q, Deng Y, Liu Y, Lu J, Liu L, et al. Loss of VGLL4 suppresses tumor PD-L1 expression and immune evasion. EMBO J. 2019;38:e99506.
40. Kriegsman BA, Vangala P, Chen BJ, Meraner P, Brass AL, Garber M, et al. Frequent Loss of IRF2 in cancers leads to immune evasion through decreased MHC class I antigen presentation and increased PD-L1 expression. J Immunol. 2019;203:1999–2010.
41. Abraham RT, Weiss A. Jurkat T cells and development of the T-cell receptor signalling paradigm. Nat Rev Immunol. 2004;4:301–8.
42. Cai M, Zhao X, Cao M, Ma P, Chen M, Wu J, et al. T-cell exhaustion interrelates with immune cytolytic activity to shape the inflamed tumor microenvironment. J Pathol. 2020;251:147–59.
43. Thorsson V, Gibbs DL, Brown SD, Wolf D, Bortone DS, Ou Yang T-H, et al. The immune landscape of cancer. Immunity. 2018;48:812–30.
44. Newman AM, Steen CB, Liu CL, Gentles AJ, Chaudhuri AA, Scherer F, et al. Determining cell type abundance and expression from bulk tissues with digital cytometry. Nat Biotechnol. 2019;37:773–82.
45. Burdett S, Stewart L, Auperin A, Pignon J-P. Chemotherapy in non-small-cell lung cancer: an update of an individual patient data meta-analysis. JCO. 2005;23:924–5.
46. Reck M, Rodríguez-Abreu D, Robinson AG, Hui R, Csőszi T, Fülöp A, et al. Pembrolizumab versus chemotherapy for PD-L1-positive non-small-Cell lung cancer. N Engl J Med. 2016;375:1823–33.
47. Gandhi L, Rodríguez-Abreu D, Gadgeel S, Esteban E, Felip E, De Angelis F, et al. Pembrolizumab plus chemotherapy in metastatic non-small-cell lung cancer. N Engl J Med. 2018;378:2078–92.
48. Rusch VW, Chaft JE, Johnson B, Wistuba II, Kris MG, Lee JM, et al. Neoadjuvant atezolizumab in resectable non-small cell lung cancer (NSCLC): Initial results from a multicenter study (LCMC3). JCO. 2018;36:8541–8541.
49. Li J-Y, Chen Y-P, Li Y-Q, Liu N, Ma J. Chemotherapeutic and targeted agents can modulate the tumor microenvironment and increase the efficacy of immune checkpoint blockades. Mol Cancer. 2021;20:27.
50. Wang M, Herbst RS, Boshoff C. Toward personalized treatment approaches for non-small-cell lung cancer. Nat Med. 2021;27:1345–56.
51. Lin P-Y, Yu S-L, Yang P-C. MicroRNA in lung cancer. Br J Cancer. 2010;103:1144–8.
52. Peng Y, Croce CM. The role of MicroRNAs in human cancer. Sig Transduct Target Ther. 2016;1:15004.
53. Cai J, Fang L, Huang Y, Li R, Xu X, Hu Z, et al. Simultaneous overactivation of Wnt/β-catenin and TGFβ signalling by miR-128-3p confers chemoresistance-associated metastasis in NSCLC. Nat Commun. 2017;8:15870.
54. Yi M, Xu L, Jiao Y, Luo S, Li A, Wu K. The role of cancer-derived microRNAs in cancer immune escape. J Hematol Oncol. 2020;13:25.
55. Van Roosbroeck K, Fanini F, Setoyama T, Ivan C, Rodriguez-Aguayo C, Fuentes-Mattei E, et al. Combining Anti-Mir-155 with chemotherapy for the treatment of lung cancers. Clin Cancer Res. 2017;23:2891–904.
56. Chen X, Ba Y, Ma L, Cai X, Yin Y, Wang K, et al. Characterization of microRNAs in serum: a novel class of biomarkers for diagnosis of cancer and other diseases. Cell Res. 2008;18:997–1006.
57. Dama E, Colangelo T, Fina E, Cremonesi M, Kallikourdis M, Veronesi G, Bianchi F. Biomarkers and Lung Cancer Early Detection: State of the Art. Cancers 2021;13(15):3919. https://doi.org/10.3390/cancers13153919.
58. Schwarzenbach H, Hoon DS, Pantel K. Cell-free nucleic acids as biomarkers in cancer patients. Nat Rev Cancer. 2011;11:426–37.
59. Kumar MS, Lu J, Mercer KL, Golub TR, Jacks T. Impaired microRNA processing enhances cellular transformation and tumorigenesis. Nat Genet. 2007;39:673–7.
60. Rottenberg S, Disler C, Perego P. The rediscovery of platinum-based cancer therapy. Nat Rev Cancer. 2021;21:37–50.
61. Fournel L, Wu Z, Stadler N, Damotte D, Lococo F, Boulle G, et al. Cisplatin increases PD-L1 expression and optimizes immune check-point blockade in non-small cell lung cancer. Cancer Lett. 2019;464:5–14.
62. Danbaran GR, Aslani S, Sharafkandi N, Hemmatzadeh M, Hosseinzadeh R, Azizi G, et al. How microRNAs affect the PD-L1 and its synthetic pathway in cancer. Int Immunopharmacol. 2020;84:106594.
63. Zeng C, Ye S, Chen Y, Zhang Q, Luo Y, Gai L, et al. HOXA-AS3 promotes proliferation and migration of hepatocellular carcinoma cells via the miR-455-5p/PD-L1 axis. Lu X-J, editor. Journal of Immunology Research. 2021;2021:1–12.
64. Xing Q, Xie H, Zhu B, Sun Z, Huang Y. MiR-455-5p suppresses the progression of prostate cancer by targeting CCR5. Biomed Res Int. 2019;2019:1–8.
65. Zheng X, Rui S, Wang X-F, Zou X-H, Gong Y-P, Li Z-H. circPVT1 regulates medullary thyroid cancer growth and metastasis by targeting miR-455-5p to activate CXCL12/CXCR4 signaling. J Exp Clin Cancer Res. 2021;40:157.
66. Aili T, Paizula X, Ayoufu A. miR-455-5p promotes cell invasion and migration in breast cancer. Mol Med Report. 2017. https://doi.org/10.3892/mmr.2017.8101.
67. Yang Q, Hou C, Huang D, Zhuang C, Jiang W, Geng Z, et al. miR-455-5p functions as a potential oncogene by targeting galectin-9 in colon cancer. Oncol Lett. 2017;13:1958–64.
68. Chen D, Xie S, Wu Y, Cui Y, Cai Y, Lan L, et al. Reduction of bladder cancer chemosensitivity induced by the effect of HOXA-AS3 as a ceRNA for miR-455-5p that upregulates Notch1. Front Oncol. 2021;10:572672.
69. Zeng C, Ye S, Chen Y, Zhang Q, Luo Y, Gai L, et al. HOXA-AS3 promotes proliferation and migration of hepatocellular carcinoma cells via the miR-455-5p/PD-L1 axis. J Immunol Res. 2021;2021:9289719.
70. Aguilar EJ, Ricciuti B, Gainor JF, Kehl KL, Kravets S, Dahlberg S, et al. Outcomes to first-line pembrolizumab in patients with non-small-cell lung cancer and very high PD-L1 expression. Ann Oncol. 2019;30:1653–9.
71. Rizvi H, Sanchez-Vega F, La K, Chatila W, Jonsson P, Halpenny D, et al. Molecular determinants of response to anti-programmed cell death (PD)-1 and anti-programmed death-ligand 1 (PD-L1) blockade in patients with non-small-cell lung cancer profiled with targeted next-generation sequencing. J Clin Oncol. 2018;36:633–41.
72. Fehrenbacher L, von Pawel J, Park K, Rittmeyer A, Gandara DR, Ponce Aix S, et al. Updated efficacy analysis including secondary population results for OAK: a randomized phase III study of atezolizumab versus docetaxel in patients with previously treated advanced non-small cell lung cancer. J Thorac Oncol. 2018;13:1156–70.
73. Gocher AM, Workman CJ, Vignali DAA. Interferon-γ: teammate or opponent in the tumour microenvironment? Nat Rev Immunol. 2021;22(3):158-72. https://doi.org/10.1038/s41577-021-00566-3.
74. Ayers M, Lunceford J, Nebozhyn M, Murphy E, Loboda A, Kaufman DR, et al. IFN-γ–related mRNA profile predicts clinical response to PD-1 blockade. J Clin Investig. 2017;127:2930–40.
75. Higgs BW, Morehouse CA, Streicher K, Brohawn PZ, Pilataxi F, Gupta A, et al. Interferon gamma messenger RNA signature in tumor biopsies predicts outcomes in patients with non-small cell lung carcinoma or urothelial cancer treated with durvalumab. Clin Cancer Res. 2018;24:3857–66.

76. Uruga H, Bozkurtlar E, Huynh TG, Muzikansky A, Goto Y, Gomez-Caraballo M, et al. Programmed cell death ligand (PD-L1) expression in stage II and III lung adenocarcinomas and nodal metastases. J Thorac Oncol. 2017;12:458–66.
77. Clark NA, Hafner M, Kouril M, Williams EH, Muhlich JL, Pilarczyk M, et al. GRcalculator: an online tool for calculating and mining dose–response data. BMC Cancer. 2017;17:698.
78. Dama E, Melocchi V, Dezi F, Pirroni S, Carletti RM, Brambilla D, et al. An aggressive subtype of stage I lung adenocarcinoma with molecular and prognostic characteristics typical of advanced lung cancers. Clin Cancer Res. 2017;23:62–72.
79. Sebaugh JL. Guidelines for accurate EC50/IC50 estimation. Pharmaceut Stat. 2011;10:128–34.

Publisher's Note

Terms and Conditions

Springer Nature journal content, brought to you courtesy of Springer Nature Customer Service Center GmbH (“Springer Nature”).
Springer Nature supports a reasonable amount of sharing of research papers by authors, subscribers and authorised users (“Users”), for small-scale personal, non-commercial use provided that all copyright, trade and service marks and other proprietary notices are maintained. By accessing, sharing, receiving or otherwise using the Springer Nature journal content you agree to these terms of use (“Terms”). For these purposes, Springer Nature considers academic use (by researchers and students) to be non-commercial.
These Terms are supplementary and will apply in addition to any applicable website terms and conditions, a relevant site licence or a personal subscription. These Terms will prevail over any conflict or ambiguity with regards to the relevant terms, a site licence or a personal subscription (to the extent of the conflict or ambiguity only). For Creative Commons-licensed articles, the terms of the Creative Commons license used will apply.
We collect and use personal data to provide access to the Springer Nature journal content. We may also use these personal data internally within ResearchGate and Springer Nature and as agreed share it, in an anonymised way, for purposes of tracking, analysis and reporting. We will not otherwise disclose your personal data outside the ResearchGate or the Springer Nature group of companies unless we have your permission as detailed in the Privacy Policy.
While Users may use the Springer Nature journal content for small scale, personal non-commercial use, it is important to note that Users may not:

1. use such content for the purpose of providing other users with access on a regular or large scale basis or as a means to circumvent access control;
2. use such content where to do so would be considered a criminal or statutory offence in any jurisdiction, or gives rise to civil liability, or is otherwise unlawful;
3. falsely or misleadingly imply or suggest endorsement, approval , sponsorship, or association unless explicitly agreed to by Springer Nature in writing;
4. use bots or other automated methods to access the content or redirect messages
5. override any security feature or exclusionary protocol; or
6. share the content in order to create substitute for Springer Nature products or services or a systematic database of Springer Nature journal content.

In line with the restriction against commercial use, Springer Nature does not permit the creation of a product or service that creates revenue, royalties, rent or income from our content or its inclusion as part of a paid for service or for other commercial gain. Springer Nature journal content cannot be used for inter-library loans and librarians may not upload Springer Nature journal content on a large scale into their, or any other, institutional repository.
These terms of use are reviewed regularly and may be amended at any time. Springer Nature is not obligated to publish any information or content on this website and may remove it or features or functionality at our sole discretion, at any time with or without notice. Springer Nature may revoke this licence to you at any time and remove access to any copies of the Springer Nature journal content which have been saved.
To the fullest extent permitted by law, Springer Nature makes no warranties, representations or guarantees to Users, either express or implied with respect to the Springer nature journal content and all parties disclaim and waive any implied warranties or warranties imposed by law, including merchantability or fitness for any particular purpose.
Please note that these rights do not automatically extend to content, data or other material published by Springer Nature that may be licensed from third parties.
If you would like to use or distribute our Springer Nature journal content to a wider audience or on a regular basis or in any other manner not expressly permitted by these Terms, please contact Springer Nature at

onlineservice@springernature.com